Variable time delays in the propagation of the interplanetary magnetic field

D. R. Weimer,[1] D. M. Ober,[1] N. C. Maynard,[1] W. J. Burke,[2] M. R. Collier,[3]
D. J. McComas,[4] N. F. Ness,[5] and C. W. Smith[5]

Received 9 October 2001; revised 10 December 2001; accepted 16 December 2001; published 28 August 2002.

[1] Simultaneous measurements of the interplanetary magnetic field (IMF) are obtained at various locations with four spacecraft, ACE, Wind, IMP-8, and Geotail. We have devised a technique whereby the exact propagation delay time between ACE, at the L1 orbit, and each of the other three spacecraft can be derived from these measurements. This propagation delay is determined as a continuously varying function of time; when this measured delay is applied to all three components of the IMF measured by ACE, they will match the other satellites' IMF to a degree that is much better than expected. However, the actual time delays can vary by nearly an hour in either direction from the expected advection delays, and the lag times have significant changes that can occur on a timescale of a few minutes. These results are interpreted as due to the effects of tilted phase fronts that are changing orientation with time. We have used the delay measurements between multiple satellites to calculate the three-dimensional orientation and temporal variations of the phase front. The best fit phase front plane usually lies within 4 R_E or less from the four-point measurements, indicating a lag resolution of a minute or less. Computer animations of the time-varying phase fronts are used to illustrate their behavior. Orientations can change on short timescales. Our findings have implications for both basic research and ''space weather'' predictions. These results give a high confidence that the same IMF that is measured near L1 will most likely impact the Earth's magnetosphere, providing ample justification for use of spacecraft data in halo orbit at L1 for monitoring the upstream solar wind prior to its interacting with the magnetosphere. However, there is strong uncertainty in the timing of the arrival of the detailed IMF structures, and these delays will need to be considered. *INDEX TERMS:* 2722 Magnetospheric Physics: Forecasting; 2134 Interplanetary Physics: Interplanetary magnetic fields; 2784 Magnetospheric Physics: Solar wind/magnetosphere interactions; 2194 Interplanetary Physics: Instruments and techniques; *KEYWORDS:* interplanetary magnetic field, IMF, space weather, Advanced Composition Explorer, ACE

1. Introduction

[2] Measurements of the interplanetary magnetic field (IMF) in the solar wind upstream from the Earth are increasingly critical for improving our understanding of solar-terrestrial interactions and for operational space weather predictions. The most practical position for upstream monitoring is at the gravitationally stable first Lagrangian (L_1) position, ~230 R_E from Earth toward the Sun. Currently, NASA's Advanced Composition Explorer (ACE) satellite operates in a halo orbit around L_1, ~35 R_E from the Sun-Earth line. Interplanetary parameters measured near L_1 are acquired about an hour in advance of terrestrial effects. While ACE measurements are extremely useful, questions have been raised concerning the degree to which measurements taken off-axis near L_1 accurately represent the IMF that interacts with the Earth's magnetosphere. Previous investigations indicate that IMF measurements taken at wide off-axis separations do not always correlate very with those observed by satellites in the near-Earth solar wind.

[3] The ISEE 3 satellite was launched in August 1978 into a wide halo orbit about L_1 to monitor approaching interplanetary structures capable of causing geospace disturbances [*Tsurutani and Baker*, 1979]. To predict whether such structures actually produce geomagnetic disturbances requires knowledge of how plasmas and fields passing L_1 correlate with near Earth values. The coherence of interplanetary parameters with distance from Earth has been studied with ISEE 3 near L_1 at solar maximum and with the WIND satellite at various distances upstream near solar minimum. Most studies have focused separately on (1) IMF and (2) solar wind density/velocity structures. The main results may be summarized as follows:

[4] In the first type of study, correlations between IMF structures observed upstream in the solar wind and near

[1]Mission Research Corporation, Nashua, New Hampshire, USA.
[2]Air Force Research Laboratory Space Vehicles Directorate, Hanscom AFB, Massachusetts, USA.
[3]NASA/Goddard Space Flight Center, Greenbelt, Maryland, USA.
[4]Southwest Research Institute, San Antonio, Texas, USA.
[5]Bartol Research Institute, Newark, Delaware, USA.

0148-0227/02/2001JA009102$09.00

Earth range from good to poor [*Russell et al.*, 1980]. Good correlations are most frequently obtained if the IMF variability is high. When the IMF variability is low, good correlations are obtained if the distance perpendicular to the propagation direction $d_{\perp}<20$ R_E [*Crooker et al.*, 1982]. *Russell et al.* [1980] suggested that the poorer correlations might reflect effects of propagating hydromagnetic structures in the solar wind or that the surface normals to planes separating magnetic fields of different orientation make large angles to the ecliptic. By comparing the fraction of good IMF obtained with ISEE 3 and Wind near L_1, *Collier et al.* [1998] showed that coherence degenerates significantly near solar minimum. Through a probability analysis of observed advection times from L_1 to Earth, they demonstrated that phase-plane tilting rather than propagating magnetic structures were responsible for many apparent low correlations. A recent analysis of IMF measurements from the Wind, IMP 8, and Geotail spacecraft suggests that phase planes have radii of curvature of $\sim$100 R_E [*Collier et al.*, 2001].

[5] *Ridley* [2000] used Wind and IMP-8 IMF measurements to estimate the uncertainty in the timing of propagation, using four different methods or assumptions to calculate phase front planes and the resulting time delays. He analyzed a number of individual events with sharp transitions where they was an unambiguous determination of the transition time between satellites, and found that the average uncertainty is 7.5–8.5 min for off-axis distances of 30 R_E, and at 100 R_E the uncertainties are 17.5–25 min. Using the total magnetic field vector to determine the front plane gave the lowest average error.

[6] *Lyons et al.* [1997] had used IMF observations from both Wind and IMP-8 in conjunction with ground-based substorm observations in order to demonstrate evidence for substorm triggering. They found [*Lyons et al.*, 1997, p. 27,039] that "spatial structure in the plane perpendicular to the Earth-Sun line critically affects whether or not a trigger is observed from a particular IMF monitor; the probability of seeing a trigger for the substorms in our study is 89% for monitors that are <30 R_E from the Earth-Sun line but only 50% for monitors 30 R_E to 56.7 R_E from the Earth-Sun line."

[7] In the second type of study, solar wind fluxes, analyzed in 6 hr segments, showed good agreement between upstream and near-Earth measurements independent of the X_{GSE} and Y_{GSE} locations of the observing spacecraft [*Paularena et al.*, 1998]. *Richardson et al.* [1998] found that the best correlations between solar wind speeds and densities were obtained during periods of high variability in the density. A change in the correlation coefficients with X_{GSE} separation suggests that the solar wind evolved significantly across the 100 R_E diameter of ISEE 3's halo orbit about L_1. When sampling intervals were reduced to the 2 hr periods used in IMF studies, plasma correlations deteriorated to values less than those found for magnetic fields. *Richardson and Paularena* [1998] used three spacecraft to find the average east-west orientation of plasma structures in the solar wind. Using an analysis of 6 hr segments, they found that the average orientation of plasma fronts is roughly halfway between perpendicular to the solar wind and the Parker spiral direction. *Coplan et al.* [2001] compared solar wind fluxes observed by the SOHO (near L_1) and Wind spacecraft at large X_{GSE} and Y_{GSE} separations. The database extended from solar minimum (1996) to maximum (2000). Better correlations were observed near solar maximum. Again the concept of planar fronts proved useful in organizing the measurements, with the average surface normal in the quadrant of the Parker spiral.

[8] *Richardson and Paularena* [2001] also used multiple spacecraft and compared correlations for both the plasma and IMF. They found a very strong dependence of correlation on spacecraft separation in the YZ plane. Scale lengths perpendicular to the flow, the distance over which the correlation decreases by 0.1, were 45 R_E for the IMF components, 70 R_E for plasma velocity and IMF magnitude, and over 100 R_E for density. Front orientations were similar for both plasma and IMF features.

[9] Using data from the Sakigake satellite at 0.8–1.0 AU, *Nakagawa et al.* [1989] found periods lasting over 2 h that they called "planar magnetic structures" (PMS), characterized by variations in the magnetic field vector that were nearly parallel to a fixed plane. The plane includes the spiral direction but is inclined to the ecliptic plane from 30°E to 85°E. *Farrugia et al.* [1990] report observations of PMS oriented at a large angle, $\sim$80°E, to the Parker spiral, interpreted as produced by draping about a high velocity, compressed plasma cloud.

[10] A complementary perspective on phase plane-propagation emerged from the analysis of electric fields detected during two rocket flights out of Svalbard in the midday magnetic local time (MLT) sector [*Maynard et al.*, 2000, 2001a]. At the times of the launches the Wind satellite was near GSM coordinates (200, 10, 25) R_E. IMF B_Z was northward during the first and southward during the second flight. In both cases B_X was the dominant component. Electric field variations in the ionosphere were compared with those in the interplanetary electric field (IEF) $E = V B_{YZ} \sin^2 \theta/2$. Here V is the solar wind speed, B_{YZ} is the projection of the IMF onto the GSM Y-Z plane, and θ is the clock angle of B_{YZ}. This representation of the IEF provides the maximum rate of component merging on the dayside magnetopause [*Sonnerup*, 1974]. Varying electric fields with similar waveforms were detected during the rocket flights and at locations Wind and IMP 8 satellites. In both instances the correlated signals were detected in the ionosphere well before expected advection times from L_1 to Earth. From the observed timing of IEF variations at Wind, IMP 8 and the approximate merging sites on the dayside magnetopause, *Maynard et al.* [2000, 2001b] estimated the tilts of phase planes that required significant rotations with respect to both the Y_{GSM} and Z_{GSM} axes.

[11] Results of these previous studies, the majority of which have been based on long-period average observations, have implications for the accuracy of space-weather predictions using monitors in L_1 halo orbits. To investigate the question of accuracy in more detail, we had taken advantage of simultaneous measurements of the IMF available from four satellites, ACE, Wind, IMP-8, and Geotail. We had found that IMF measurements from all four satellites agreed much better than anticipated, when the advection lag was allowed to vary. Significant and highly variable changes in the delay times between the specific features observed at each satellite occur on timescales of

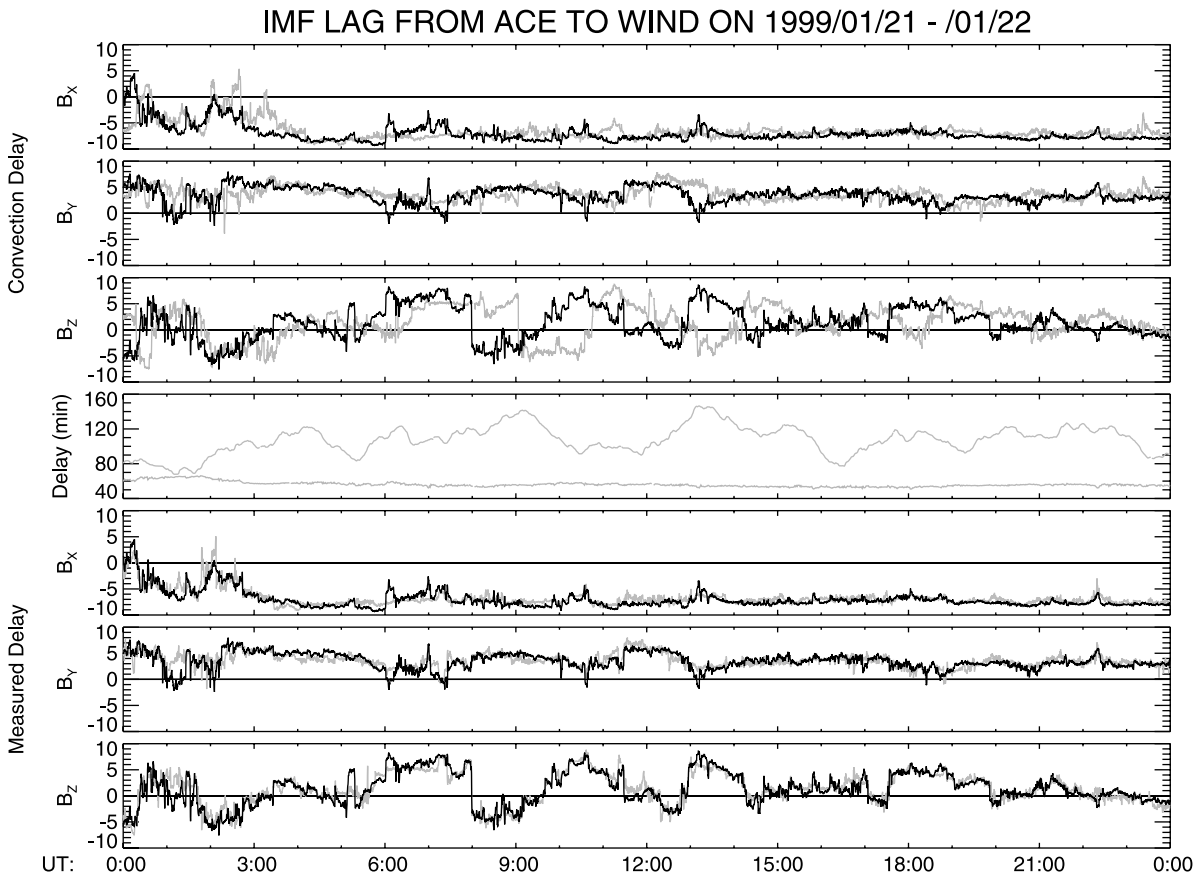

Figure 1. Interplanetary magnetic field (IMF) measured with the ACE and Wind satellites on January 21, 1999. The black lines in the three top and bottom panels show the ACE data. The green lines in the top three panels show the Wind data, with the measurements shifted in time according to the value of the advection delay, shown as the green line in the middle panel. The blue lines in the bottom three panels show the same data from Wind shifted in time by a variable amount that results in the best agreement with the ACE data. The lag time that produces this agreement is called the "measured delay," and is shown as the blue line in the middle panel. See color version of this figure at back of this issue.

minutes. This paper reports our initial findings concerning variable time delays.

2. A New Technique for the Accurate Determination of Time Delays

[12] The importance of time delays is illustrated in Figure 1 which shows IMF measurements taken by ACE and Wind on January 21, 1999. Spacecraft locations are given in Table 1. The black lines in the top three panels of Figure 1 show the three GSE components of the IMF vector measured by ACE. In this and subsequent graphs, time lines on the horizontal axis are referenced to the times of measurements at ACE. In order to compare them with Wind measurements, it is necessary to compensate for time delays in solar wind propagation. The green line in the middle panel shows this advection/convection delay, calculated by dividing the separation distance along the GSE X axis by the X component of the solar wind velocity. The velocity was measured by the Solar Wind Electron, Proton, and Alpha Monitor (SWEPAM) on ACE [*McComas et al.*, 1998]. In this particular case the computed convection delay is relatively stable, at ~60 minutes. The green lines in top three panels show a superposition of the three components of the IMF vector measured by Wind, employing this convection delay. For example, at the 0800 UT position on the graph, IMF measurements from ACE were obtained at 0800 UT, and the IMF data from Wind were actually measured about an hour later at ~0900 UT. With this lag, the data agree poorly, and appear to have a negative correlation. However, when the Wind data are shifted in time by the proper lags they generally agree very well with the ACE data stream, as shown in the bottom three panels (although there are times where the match is not perfect). The ACE IMF measurements are again

Table 1. Positions of the Satellites for the Three Cases

Date	Spacecraft	GSE Position (R_E)		
		X	Y	Z
Jan. 21, 1999	ACE	236.0	32.9	13.6
	Wind	−13.1	−51.5	12.5
April 29, 1999	ACE	224.5	−22.9	−16.4
	Wind	53.0	−19.3	−11.3
	IMP-8	15.5	29.4	−26.4
	Geotail	12.1	17.0	−2.9
June 6, 1999	ACE	231.1	34.5	−13.8
	Wind	205.4	−21.1	−8.2
	IMP-8	34.6	−10.4	−18.0
	Geotail	22.3	8.4	−3.0

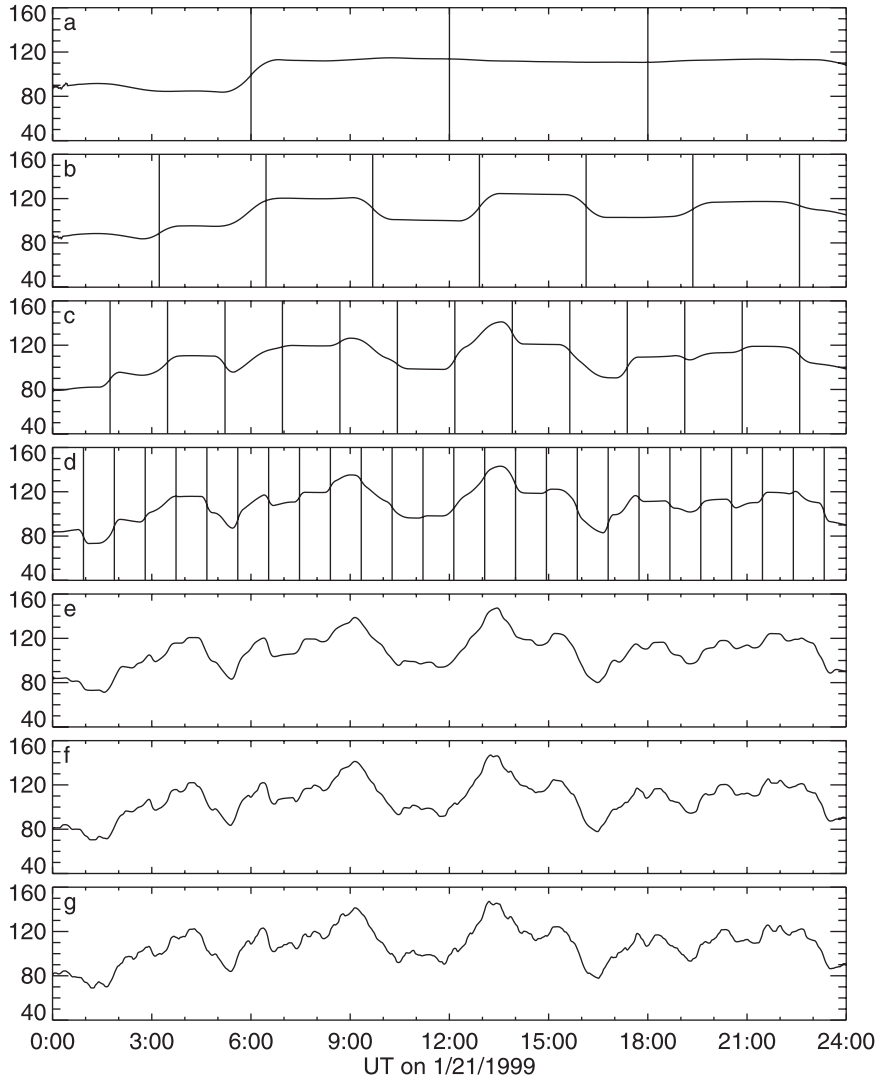

Figure 2. Example of the measured time delay as it evolves through the first seven steps of the calculation. The IMF data for this same interval are in Figure 1. The delay function is initialized with the advection value. In the first step (a) the entire interval is divided into 6 h segments, marked with the vertical lines, and the best delay offset from initial value is determined in each segment. The process is repeated, with the segment duration multiplied by 7/13 at each subsequent step while also increasing the resolution of the delay offset in each step. For clarity the segment boundaries are not shown after the first four steps.

shown in black, and this time the Wind measurements are in blue. The actual lag time used to obtain this match is shown in blue in the middle panel. We refer to the lag that gives the best match between the two sets of vector measurements as the measured delay. The lag is not fixed. As seen in the graph it varies, ranging from ~60 min at 0130 UT to almost 150 min after 1300 UT. At this time it took the IMF 1.5 hr longer than expected to propagate from ACE to Wind. Note that the single variable lag usually brings the features of all three components of the IMF into agreement.

[13] Such large variability in advection delays seriously impacts our ability to understand magnetospheric interactions and predict space weather. We attribute the difference between the expected and actual advection delay times to planar IMF phase fronts whose surface normals are tilted at some angle with respect to the direction of the solar wind velocity vector. The positions of ACE and Wind at the midpoint of this interval, listed in Table 1, indicate that they had a larger separation in the Y_{GSE} direction (~84 R_E), which caused the tilted phase plane to reach Wind at the late time. As noted above, the concept of tilted phase planes is not new [i.e., *Collier et al.*, 1998; *Maynard et al.*, 2000, 2001b; *Coplan et al.*, 2001], and *Maynard et al.* [2000, 2001b] found that the planes are also tilted in the XZ plane when a significant B_X is present. The fact that phase-front orientations and resulting lags varied continuously as functions of time was unexpected, with significant changes occurring within a few minutes. Variable time lags were not immediately obvious, and our method for calculating delays evolved during the research process. Our initial objective was to compare the IMF measurements of four satellites. It soon became apparent that measurements from

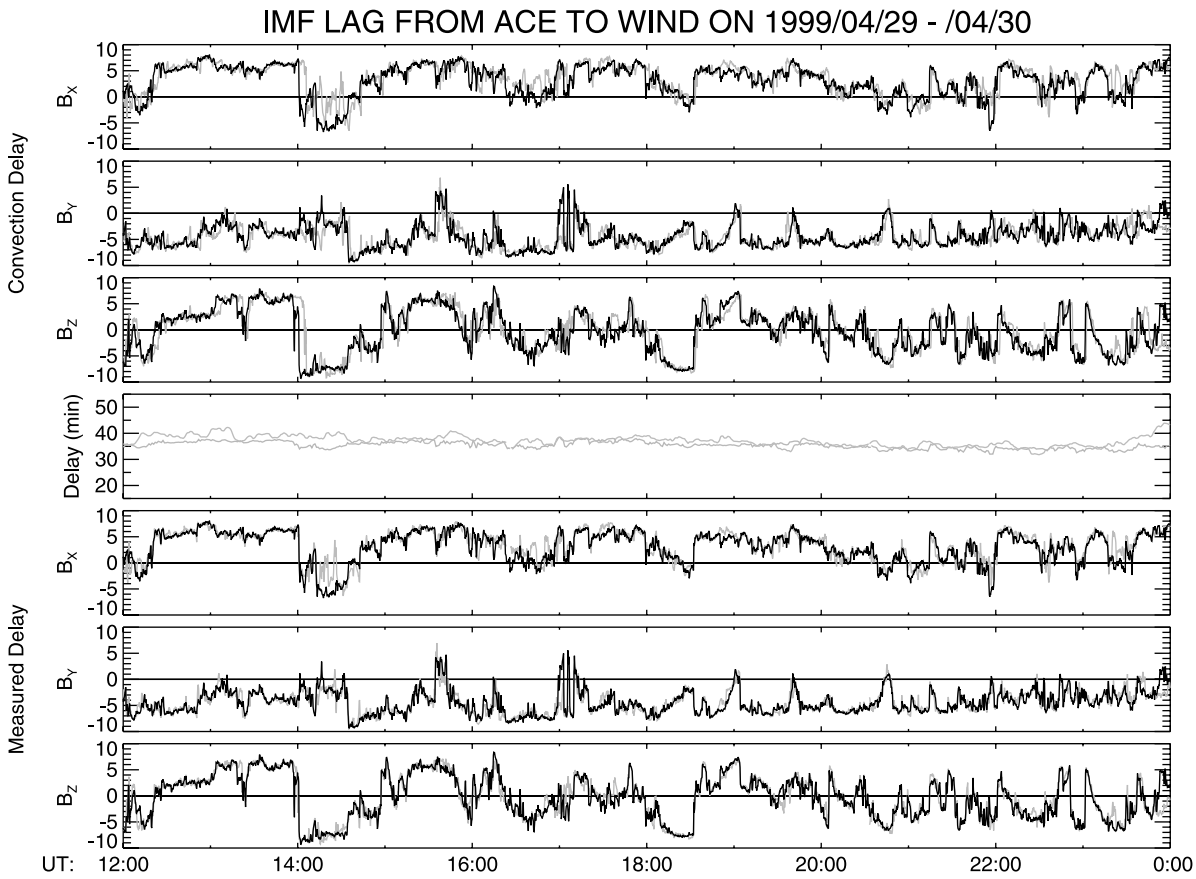

Figure 3. IMF measured with the ACE and Wind satellites on April 29, 1999. The format is the same as in Figure 1. See color version of this figure at back of this issue.

all four satellites appeared to agree very well, with all significant features present, but only if the timings were adjusted. The first attempt to calculate the proper lags used fixed-width time intervals, of ~90 min, calculating the best lag for each interval. The resulting lag-versus-time graphs had stair-step forms with discontinuities at each step that seemed unnatural.

[14] Rather than describe each step in our development, here we only outline the final algorithm for calculating the time lags. The process begins by dividing selected time intervals into sections, adjusting the lag time in each section from the previous value, and repeating the process using smaller and smaller divisions, while simultaneously decreasing the magnitude of the adjustments and improving the resolution. The time period shown in Figure 1 is used for purpose of illustration. Several steps in the sequence appear in Figure 2. To start the sequence, the advection delay time for the entire interval was used as the initial value of the measured delay function. This value was assigned to each of the 16 s resolution of ACE measurements of the IMF.

[15] The initial interval was divided into 6 h segments, with the last segment extended to the end if the interval was not an even multiple of 6 h. An error value was calculated for each segment as follows. The time line at ACE is used as a fixed reference. The value of the delay function at each step is added to that time to obtain the delayed time at the target satellite. This time is in the future if the delay is positive. The ends of the segment may well be outside the range of the 6 h period under consideration. An interpolation of all IMF vector components that were measured at the target is used to obtain the IMF at the delayed times, one vector for each measurement in the original time series at ACE. The error is calculated by adding the square of the difference between each of the three vector components, accumulating the sum for every ACE data point in the segment.

[16] For each segment a constant delay adjustment was found such that, when added to the previous delay function in that segment, the error between the IMF measured by ACE and the target satellite was minimized. This best delay offset was found by trying several possible values within an allowed range of offsets. For the initial segment period of 6 h, the tested offsets were in the range of −54 m to +54 m, or ±15% of the period. If the two best offsets were different by more than a desired resolution of 4.5 m (1.25% of the period), then several values between these best values were tried (this procedure is similar to a binary search). In essence this procedure finds the delay value that minimizes the least squares error between the three-vector series. After the optimal delay offset is found for a segment, the delay curve obtained with this offset replaces the original estimate for the data segment. The results after this first step are shown in Figure 2a. The boundaries of the 6 h segments are shown on

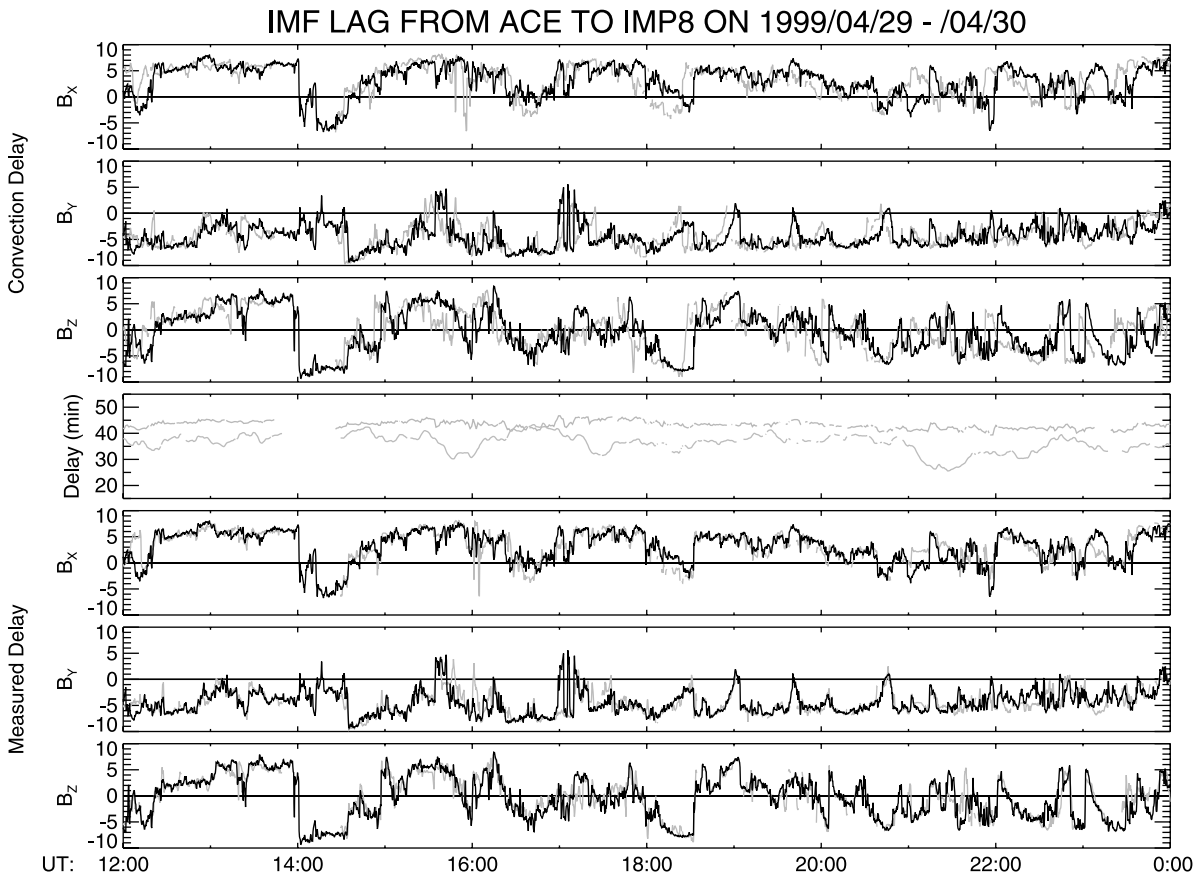

Figure 4. IMF measured with the ACE and IMP-8 satellites on April 29, 1999. The format is the same as in Figure 1, with the green and blue lines now showing the IMP-8 data. The gaps in the green and blue lines indicate where there were gaps in the IMF measured with IMP-8. See color version of this figure at back of this issue.

the illustration with the vertical lines. Discontinuities at the boundaries were smoothed with boxcar averaging.

[17] The same procedure was repeated with segments that are 7/13 times the original length, or approximately 0.5385 h, with the results shown in Figure 2b. The range of offsets tested was again ±15% of the period, now ±29.1 m, and the resolution 2.42 m. The process was repeated a total of nine times. The results of steps 3 to 7 are shown in Figures 2c to 2g. After Figure 2d the segment boundaries are not shown for clarity, and the last two steps are not illustrated since the changes are not readily perceptible to the eye. The duration of the final segment is 2.54 m. After the sixth step the delay resolution is fixed at 8 s.

[18] Some elements of this procedure were found by trial and error. The amount of detail or structure in the resulting delay function is sensitive to changes in the 15% factor. If it increased above 20%, the resulting delay fluctuations appeared unnatural. At one extreme, this routine can incorrectly match up IMF features with lag times of hours if it is not given reasonable constraints. On the other hand, if the allowed lag adjustments are decreased then the algorithm is not able to shift the delay time by a sufficient amount to match IMF structures that are easily visible to the eye. The original 6 h period was used so that the initial delay adjustment is approximately one hour, as required for extreme cases such as the one illustrated. Originally, segment periods were simply divided by two in each step, which sometimes resulted in unnatural features where boundary locations were aligned on sequential steps. The 7/13 factor insured that boundaries in one step usually would not match up with boundaries in other steps.

[19] Several other details are worth noting. Conventional convolution techniques for determining lag times do not work, first because they must match three-component vectors, and second, lag times are not fixed throughout the interval. Additionally, the technique must work robustly when there are gaps in the measurements, as shown below. In our method, IMF values at the target satellite obtained by interpolation are not used in computing the total square error if the times fall within a gap in the original data. The average square error is actually used, dividing by the number of valid data points, to compensate for missing data. If at some point the number of invalid (within gaps) data points exceeds the number of valid points in a segment, then the delay function within that segment remains unchanged from its previous value. We do not claim that this method is necessarily the only and best algorithm for calculating the variable time delays, but it does appear to function correctly most of the time. It is not fool proof, as some adjustments in the parameters which might help the algorithm better match obvious features in some cases might cause it to fail in other cases, by matching up

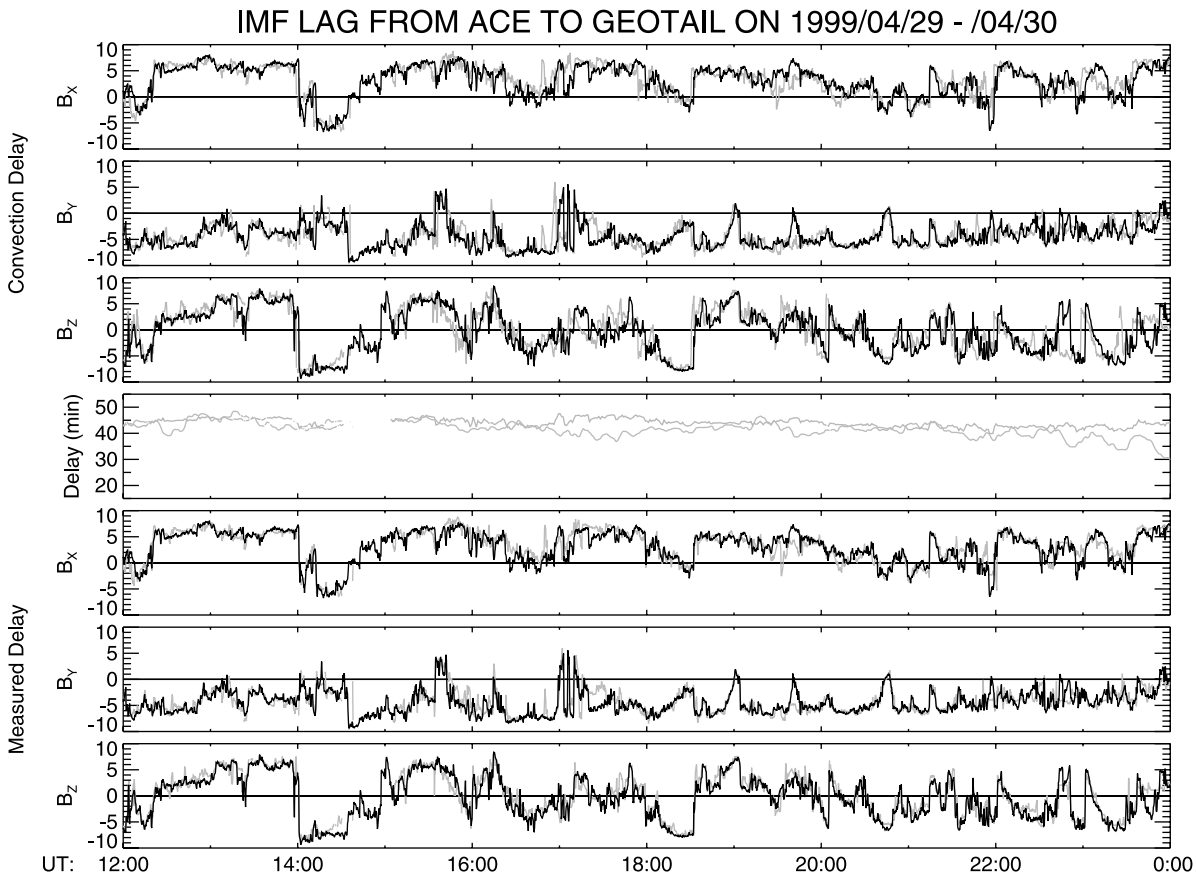

Figure 5. IMF measured with the ACE and Geotail satellites on April 29, 1999. See color version of this figure at back of this issue.

random noise fluctuations. The algorithm's performance is weakest when the IMF is relatively constant with small fluctuations.

3. Four-Satellite Comparisons

[20] Our delay calculation technique has been applied to cases when solar wind/IMF measurements are available from the ACE, Wind, IMP-8, and Geotail at the same time. The sampling periods of the IMF data used here are 16.0, 3.0, 15.36, and 3.05 s from the four satellites, respectively. The 16 s data from ACE (Level 2) are available for nearly the entire period since operations began in early 1998. The algorithm was initially developed using coarse, but readily available Key Parameter, data from the other satellites, with sampling periods of 61 to 92 s. Only recently have high-resolution (3 s) IMF data from Wind become available to us, but only up to the period through the end of July 1999. For the cases shown here, higher resolution IMP-8 and Geotail data are likewise used. The 3 s data are smoothed with a 5-box sliding average before interpolation and comparison with the 16 s data due to their higher Nyquist frequency.

[21] The time lag calculations are shown next for two of our four-satellite cases. Figures 3–5 show results from the first case spanning the period 1200 to 2400 UT on April 29, 1999. The format is identical to that of Figure 1, where the time axes on each of the three charts is referenced to IMF observations at the ACE satellite, shown with the black lines. As in Figure 1, the middle plot shows both the convection and measured delays, with green and blue lines, and the time delayed target IMF data are shown in the upper three and lower three panels with superimposed green and blue lines. Breaks in the green and blue lines on these graphs, especially IMP-8 results, indicate gaps in the original data.

[22] The results for the delay times at Wind in Figure 3 are quite different from those in Figure 1, as the measured and convection delays are similar. The reason is clear from the satellite positions indicated in Table 1, which show that Wind and ACE are not widely separated in the Y_{GSE} and Z_{GSE}. In contrast, the IMP-8 (Figure 4) and Geotail (Figure 5) lags show more significant differences between the measured and advection delays. IMF signals arrived at IMP-8 almost 20 m ahead of schedule. As indicated in Table 1, IMP-8 is the farthest from ACE in the combined Y-Z direction. If the lags are due to tilted phase fronts, then the greater the separations are perpendicular to the Sun-Earth line, the greater the discrepancy between the delays.

[23] Figure 6 shows an example of IMF structure at high resolution. Measurements from all four satellites are superimposed for the 1 hr interval 2000–2100 UT, referenced to ACE, and using measured lags for the other three. The lines are colored to distinguish between the four, using black for ACE, red for Wind, green for IMP-8, and blue for Geotail. Note that there are 10 m between the major abscissa divisions and only 2 m between the minor tick marks. There are small-scale features of $\sim$1 m or less that match at all four satellites even though the Y separation distances

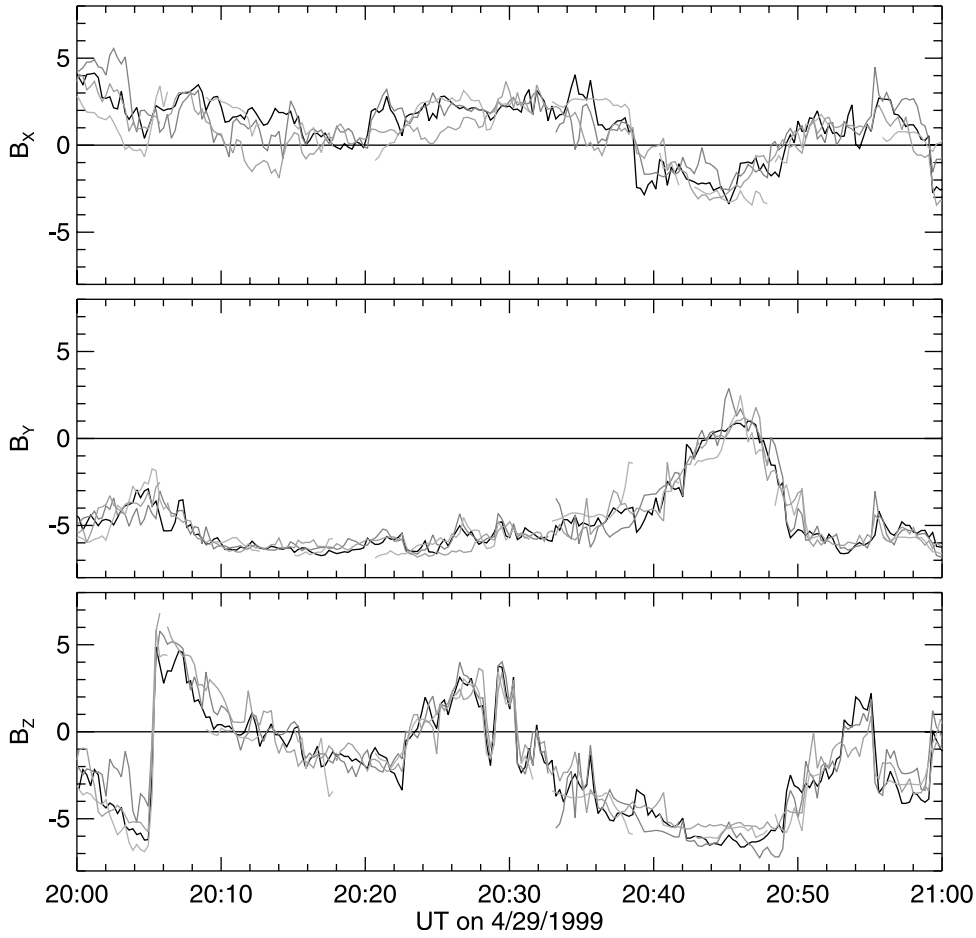

Figure 6. High-resolution graph of the IMF measured with all four satellites for a one hour interval on April 29, 1999. The data have been shifted according to the ''measured'' time delays, and are plotted on the same timescale as the ACE data, which are not shifted. The black, red, green, and blue lines show the data from ACE, Wind, IMP-8, and Geotail respectively. See color version of this figure at back of this issue.

exceed 50 R_E. The period near 2030 UT is particularly noteworthy. There are matching structures that would not be fully resolved with sampling periods >16 s or if delay calculation did not have a similar accuracy. Such detail can be found in almost any time period chosen, and it is useful to know that IMF variations on a timescale of a minute are often coherent over Y_{GSE} separations of $\sim$40 R_E.

[24] The second case, spanning the period 1200–2400 UT on June 25, 1999, is shown in Figures 7–9. There are larger differences between the measured and convection delays with all target satellites due to their varied Y-Z separations, as indicated in Table 1. Variations in lags of $\sim$20 m are common, and the sign of the actual delay with respect to the convection lag could change in minutes. Often time delays measured between ACE and the other satellites have very similar variations. As demonstrated in the next section there are differences between them that depend on the relative positions of the spacecraft and the orientations of the phase front plane.

4. Phase Front Orientation in Three Dimensions

[25] Two dimensional phase front orientations were derived from observed time lags by *Collier et al.* [1998, 2000]. *Coplan et al.* [2001] also used three satellites to derive phase fronts in three dimensions, using lags of solar wind (plasma) flux averaged over 2 and 6 h periods. Here we calculate phase front orientations that vary on timescales of minutes, using four satellites. Normally, three satellites are sufficient to derive a plane. While any three points will always fit a plane, this does not ensure that the plane has physical significance. Using four satellites provides a reality check for determining how well relative lags at locations of the four satellites agree with a planar structure. The short answer is that they generally fit very well.

[26] The method used to determine orientations of phase fronts proceeds as follows. As all measured lag times are referenced to the time line at ACE, for each of the three target satellites the lag time from ACE is multiplied by the solar wind velocity measured at ACE at that instance. The resulting distances tells how far the plane must move along the velocity vector to get from ACE to each satellite. Each of the three satellites is then moved backwards along this vector to a ''virtual'' position, starting from where they were located at the moment when the IMF from ACE reaches them (the UT at ACE plus the measured lag times). All three components of the velocity vector are used for this trans-

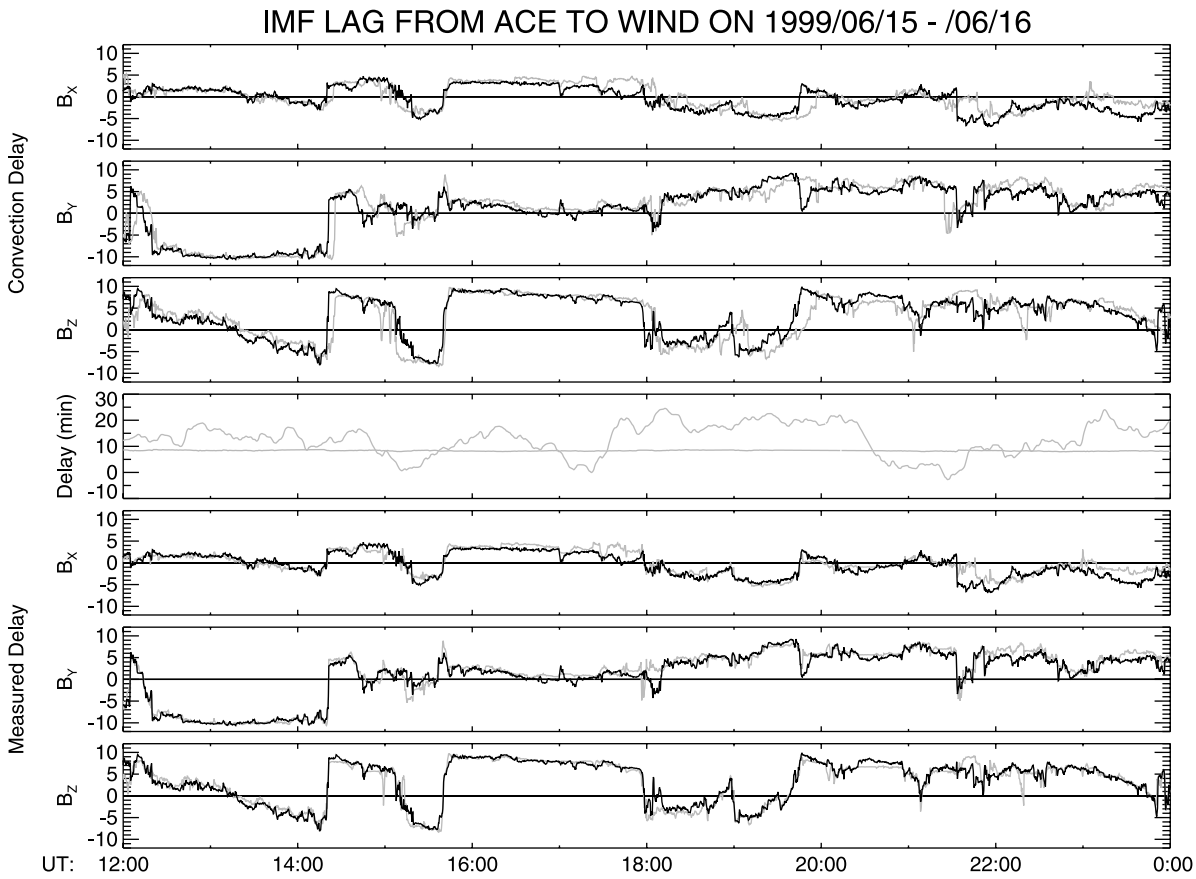

Figure 7. IMF measured with the ACE and Wind satellites on June 15, 1999. See color version of this figure at back of this issue.

lation. The resulting four points in space are then fit to a plane described by the equation

$$ax + by + cz + d = 0. \quad (1)$$

The constants a, b, and c are direction cosines that satisfy the criteria

$$a^2 + b^2 + c^2 = 1 \quad (2)$$

and d is the distance from the plane to the origin. The direction cosines also describe a unit vector that is normal to the plane. Equation (1) is solved for the four points for a least squares error fit that minimizes the distance of all points from the solution plane, using the simplex method [*Press et al.*, 1986].

[27] We have developed a computer visualization program that takes the results of time delay calculations, carries out the above plane-fitting calculations, and show a simple three-dimensional view of how the phase plane is orientated at a given moment. Example results are contained in Figure 10, where the top four panels show different views of the same configuration at 1829 UT on April 29, 1999. Four spherical points, labeled A, W, I, and G, mark the relative locations of the spacecraft after the translations described above. The semi-transparent, gray surface represents the phase plane. It has been clipped to the edges of the viewing region extending from -50 to $+90$ R_E in the X direction and from -50 to $+50$ R_E in the Y and Z directions. If there were no differences between convection delays and the measured lag times from ACE, the phase plane would be perpendicular to the X axis.

[28] An additional complexity has been introduced to the calculations described above to conform to our geocentric bias. The position of ACE was shifted forward to an X coordinate $+40$ R_E, upstream of the bow shock, and the virtual positions of the other satellites were adjusted accordingly. This way the Earth could be inserted into the picture (small blue sphere) to serve as a reference point. The different views in Figure 10, particularly where the plane is viewed from the edge, show that all four satellites do indeed fit a common plane very well. We find it difficult to make much sense of the time delay variations without such images.

[29] Time lapse animations of this three-dimensional visualization have been produced for the full duration of the cases presented in Figures 3–5 and 7–9, and are provided as Animations 1 and 2 (see HTML version of this article at http://www.agu.org). Watching how phase planes change orientation with time provides valuable insight on how well the four satellites fit a common plane, and how they all move in a coordinated manner consistent with the phase plane changes. Notable information is also gained by watching how the IMF vector changes in relationship to the measured phase plane orientation. These changing orientations must be considered for understanding magnetospheric interactions with the IMF. Figure 10 and Animations 1 and 2 include fixed-length arrows at the location of the ACE satellite

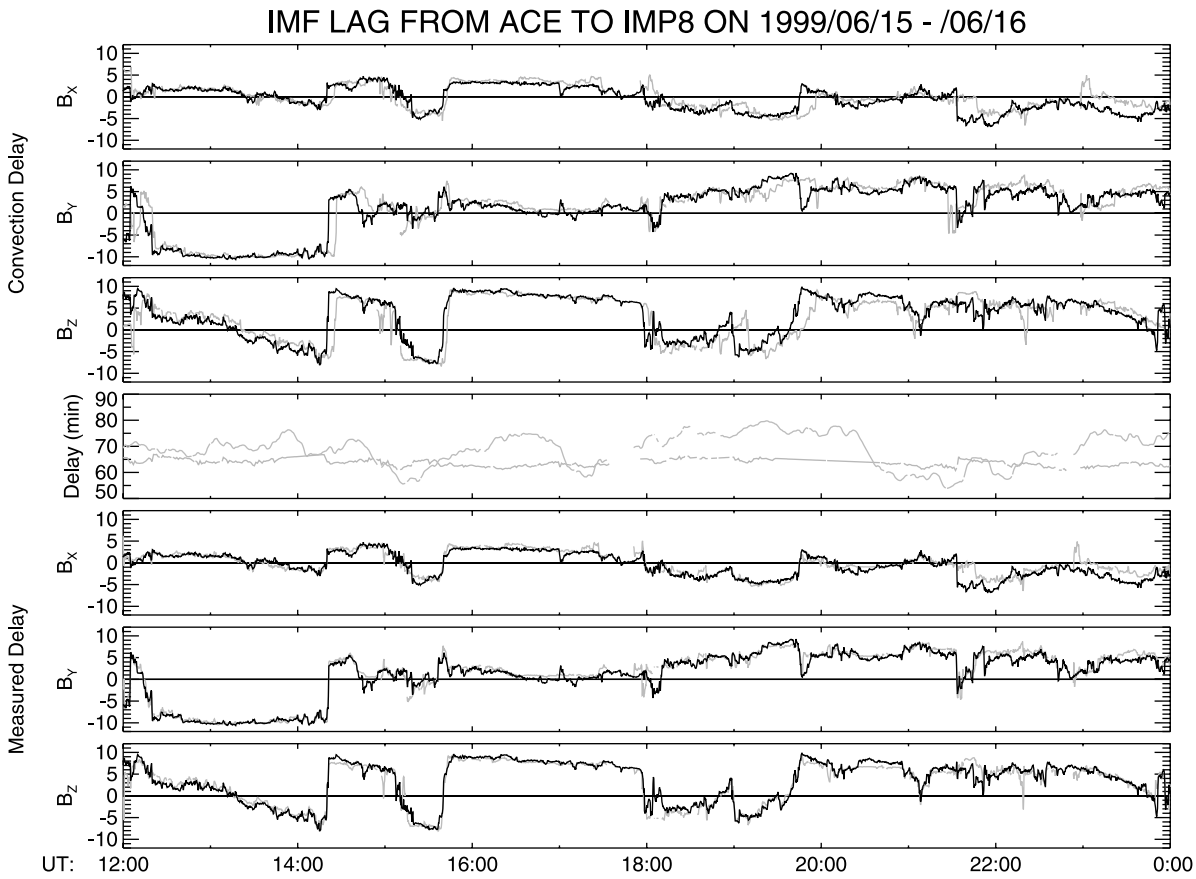

Figure 8. IMF measured with the ACE and IMP-8 satellites on June 15, 1999. See color version of this figure at back of this issue.

indicating the orientation of the IMF measured by ACE. We note that the IMF vector often, but not always, lies on or near the phase plane. At abrupt changes in the IMF direction the vector may lie within the phase plane both before and after the change while the phase plane remains nearly the same. This characteristic is illustrated in the bottom four panels of Figure 10, which shows different views of the configuration at 1839 UT, 10 m after the time considered in the top panels. The IMF underwent a significant change in direction, yet remained within the phase plane at nearly the same orientation as before. Similar IMF transitions have been examined at high resolution, and some are confirmed to be tangential discontinuities. Rotational discontinuities are also present in the IMF [*Turner and Siscoe*, 1971].

[30] Based on the tendency seen in Animations 1 and 2, that the IMF vector lies in or near the phase front, it appears that a minimum-variance analysis [*Sonnerup and Cahill*, 1967; *Sonnerup and Scheible*, 1998] should give an indication of the phase front's orientation. A minimum-variance analysis was used by *Farrugia et al.* [1990] to deduce the orientation for one event, and *Ridley* [2000] showed that it can be used to reduce uncertainty in propagation times. We have had some success using the minimum variance technique, with ACE data alone, to predict the phase front orientation angles that are measured with our 4-satellite technique. The minimum variance technique itself is prone to some uncertainty, and the accuracy can depend on arbitrary choices of how many data points to use and the criteria for rejecting indeterminate eigenvectors. Using the results of 4-satellite cases, where the correct answers are known in advance, is essential to optimizing the minimum variance parameters and gaining confidence in the results. The details of these findings will be reported in a separate paper.

[31] Graphs of phase-plane orientations as a function of time for both cases are shown in Figures 11 and 12. The three upper panels show the angles of the planes with respect to the X, Y, and Z axes, derived by taking the arcsine of the a, b, and c parameters. The values of a and the X tilt are always positive. A flat phase front with no time delay differences has the direction cosine a = 1, as the plane's normal is aligned with the X axis, and the plane itself is tilted 90 degrees from X. Both Y and Z angles are zero in this case. Variations from these values correspond to tilted planes. Substantial directional changes are seen with timescales of the order of 10 min. Figure 12 is more interesting as it corresponds to a case with consistently larger time delay differences and hence large tilt angles. The tilt in the Z direction can be substantial, over 60 degrees at times, as shown in Figure 10. From what we have observed in this and other cases, substantial tilts in the Z direction are not uncommon, while the Y tilt tends to be more moderate. In comparing Figure 12 with Figures 7–9, we note that the Z tilt correlates inversely with the lag time to the Geotail satellite, which was the farthest away from ACE in the Z direction. At the same time there is a

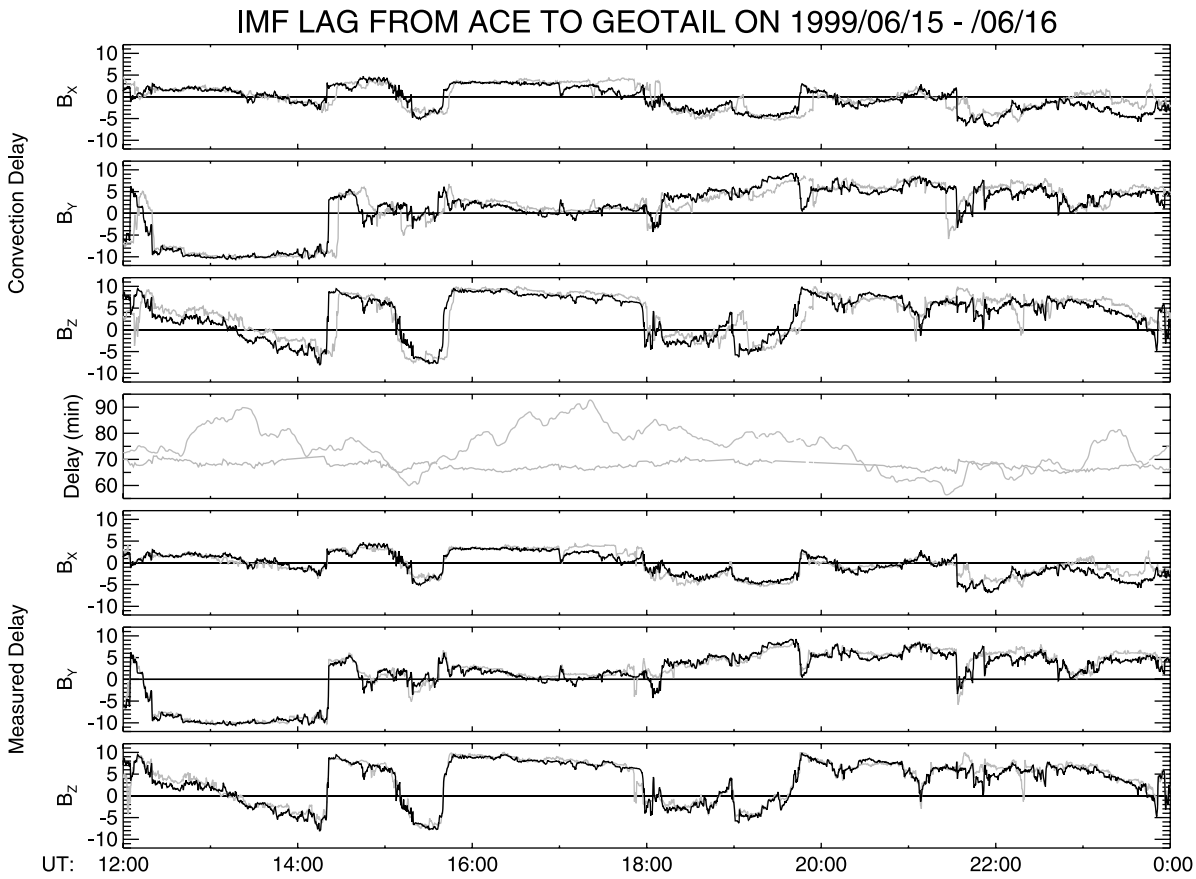

Figure 9. IMF measured with the ACE and Geotail satellites on June 15, 1999. See color version of this figure at back of this issue.

similarity between the Y tilt angle and the time delays to Wind and IMP-8.

[32] Finally we turn our attention to the bottom panels in Figures 11 and 12, labeled RMS Error, R_E. This graph shows the square root of the mean squared distance from each satellite to the best fit plane, the value minimized in the fitting procedure. It measures how well the positions of the four satellites, after lag translations, fit onto a common plane. Often this error is near zero, indicating a perfect fit. Even with degraded fits, the RMS error is rarely >4 R_E, the approximate distance that the solar wind travels in about one minute. For visual reference, the spheres in Figure 10 representing the satellites are 4 R_E in diameter. To obtain these kinds of results it is necessary to have the time lags measured to a resolution much better than 1 minute, as we have done here. To verify that the good planar fits are not accidental, we have added random noise to the measured delay values, on the order to 2 to 4 minutes, with the result that good planar fits are destroyed and the angle and error graphs become very noisy. We can also see in Figure 11 that the error increases at ~1400 UT, the same time where gaps appear in the IMP-8 and/or Geotail IMF measurements. Much of the RMS error depicted on these graphs may also be due to wavy or spherical deformations in the phase fronts, as discussed by *Collier et al.* [2000].

[33] The error calculations verify that lower errors are obtained if both the Y and Z components of the solar wind velocity, rather than X alone, are included in the satellite position translations. Fluctuations in the velocity vector cause the satellite positions in Animations 1 and 2 to shift back and forth slightly in the Y and Z directions, and the positions of the satellites in Figure 10 therefore do not match the exact locations given in Table 1. With the translation of ACE to X = 40 R_E, its position is affected by the off-axis velocity fluctuations much more than the other three. The planar fit errors also indicate that better fits are obtained when the aberration of the solar wind, due to the Earth's orbital motion, is included in the Y component of the velocity vector. The aberration component is included in the results shown here, and it causes the virtual position of ACE to be shifted by about 15 R_E.

[34] *Russell et al.* [2000] asserted that there may be a time tagging offset error of about 70 s in the IMP 8 data, which has led to some concerns within the community. If such an offset existed, then the position of IMP 8 in our results would have been consistently shifted about 5 R_E in one direction. While we have not specifically searched for an error in the IMP 8 timings, such an offset is not seen in our three-dimensional animations, and the errors in the planar fits would have been larger.

5. Discussion and Summary

[35] We have demonstrated that the propagation time of the IMF from an upstream monitor at L_1 may have significant and highly variable differences from the lag times that are

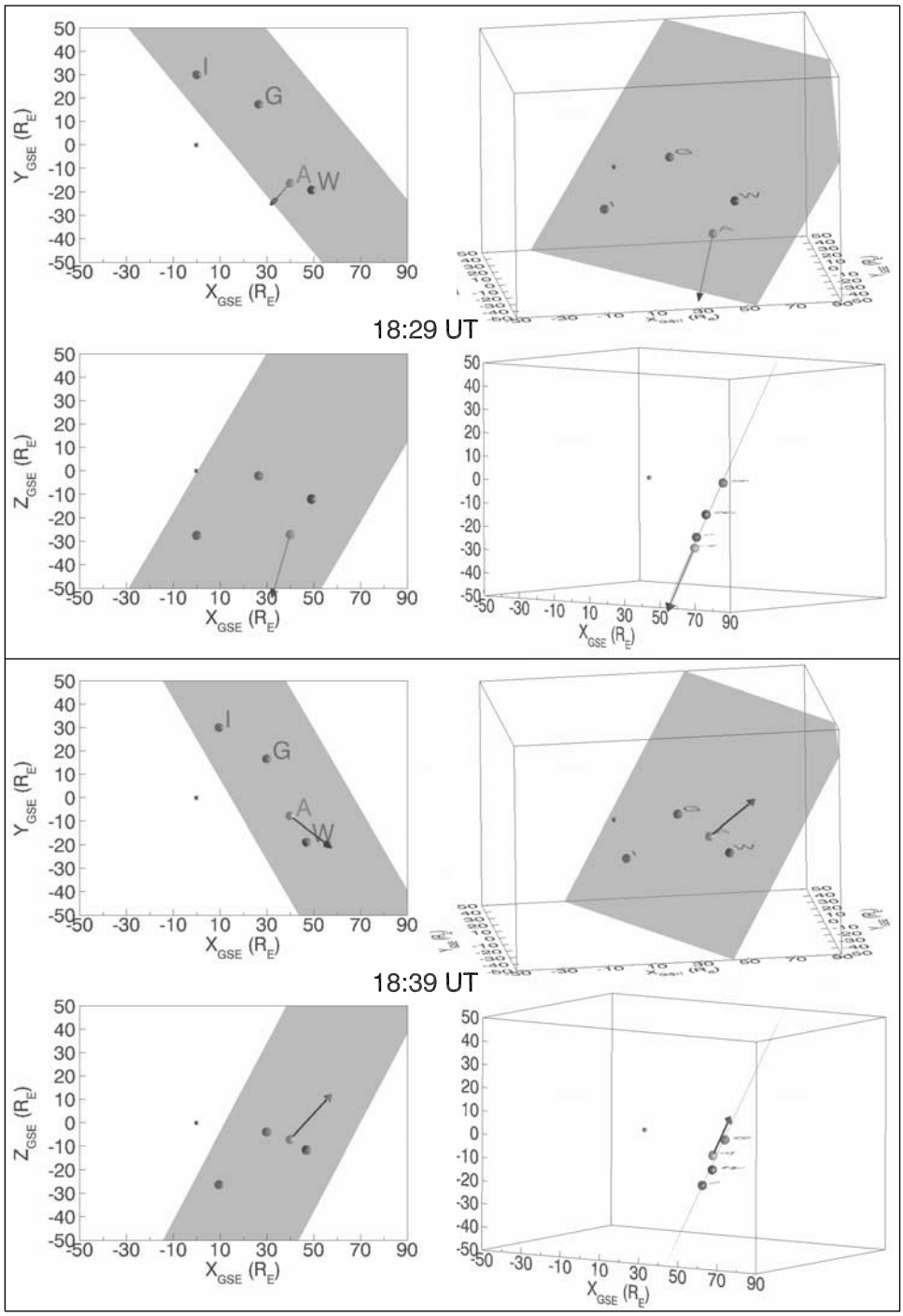

Figure 10. Three-dimensional views of the IMF phase plane orientation at two moments in time on April 29, 1999. The top four pictures show the phase plane from different viewpoints at 1829 UT, and the bottom four pictures show the same views 10 min later, at 1839 UT. The four colored spheres show the "virtual" locations of the four satellites, with the ACE satellite shifted forward up to X = 40 R_E and the others shifted according to the measured delay times and solar wind velocity, compensated for the ACE shift. All shifts are along the velocity vector, measured at ACE. The spheres are labeled with the first initial of each satellite. These spheres are drawn with a diameter of 4 R_E. For reference, a blue sphere representing the Earth is shown at the origin. The arrow at the ACE location has a fixed length and points in the direction of the IMF vector measured at ACE. The phase plane orientation remains nearly the same while the vector reverses direction. See color verion of this figure at back of this issue.

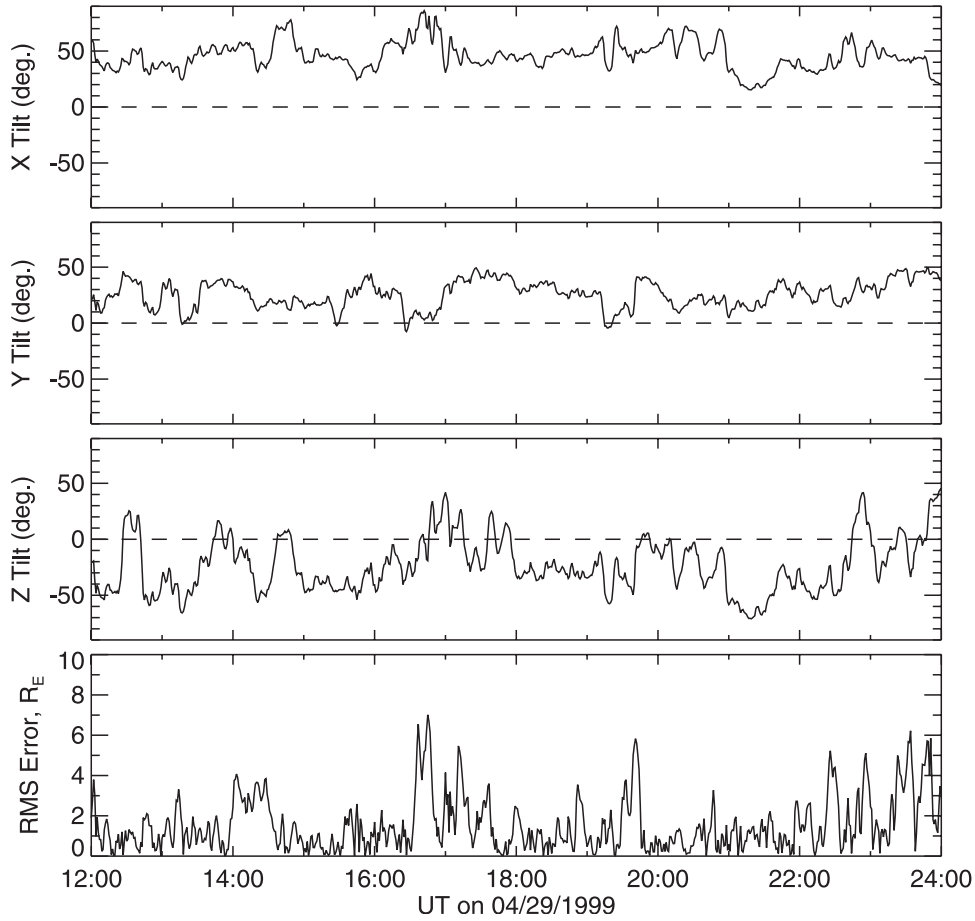

Figure 11. Graph of IMF phase plane orientation as a function of time for the case on April 29, 1999. The top three panels show the angle of the phase plane with respect to the GSE X, Y, and Z axes. The bottom panel shows the root mean square error for the fit of the four virtual satellite locations to a plane.

calculated by using a simple propagation in the GSE X direction at the solar wind velocity. We have demonstrated a method to measure the actual propagation delay time from ACE to other satellites in the solar wind. A high temporal precision is obtained, which could not otherwise be achieved by conventional convolution techniques. This method has been used with four satellites to show that the results are consistent with nearly planar, tilted phase fronts, where the tilt angles vary on timescales of minutes.

[36] The primary objective of this paper is to present these concepts and establish familiarity to them within the community. Additional, more detailed work can then follow, such as using a number of other four-satellite cases to better understand how often the phase planes are tilted and to what degree. Further study should concentrate on how well the IMF correlates from one satellite to another as off-axis separation increases, also as a function of scale size. ACE and Wind data alone are suitable for this study, but require applications of the technique presented here.

[37] The impression gained from this work suggests that, with proper time delay adjustments, the IMF correlations between different observation points are much better than expected. Thus, the probability is very high that the IMF measured at L_1 will impact the Earth's magnetopause. The important question concerns exactly when. Several implications follow from these findings. The first concerns the response time of the magnetosphere and ionosphere to IMF variations. *Ridley et al.* [1998] estimated that the delay time for ionospheric convection to begin reconfiguring after an IMF change impacts the magnetopause is ~8 minutes. It then takes about 12 more minutes to fully alter the convection pattern. *Maynard et al.* [2001a] showed that the 8 min reconfiguration delay was largely spent reversing the polarity of the cusp-mantle system of field-aligned currents. We note that the uncertainties in measurements reported by *Ridley et al.* [1998] were nearly as large as the average values. If the uncertainties reflect unknown planar tilts, using the techniques described here would likely reduce response-time variability considerably. Additionally, *Maynard et al.* [2001b] showed that tilted phase fronts impact the northern and southern merging regions of the magnetosphere at different times. As a result, different regions of the ionosphere in the same hemisphere may exhibit different lag times. With our more advanced phase front calculation tools it will be possible to make further progress in this subject.

[38] Another area of impacted research concerns the timing of external substorm triggers. *Lyons et al.* [1997] and others argue that magnetospheric substorms are triggered by northward turnings of the IMF. This hypothesis has been often disputed on the basis of anecdotal cases where the timings between IMF variations and substorm onsets were

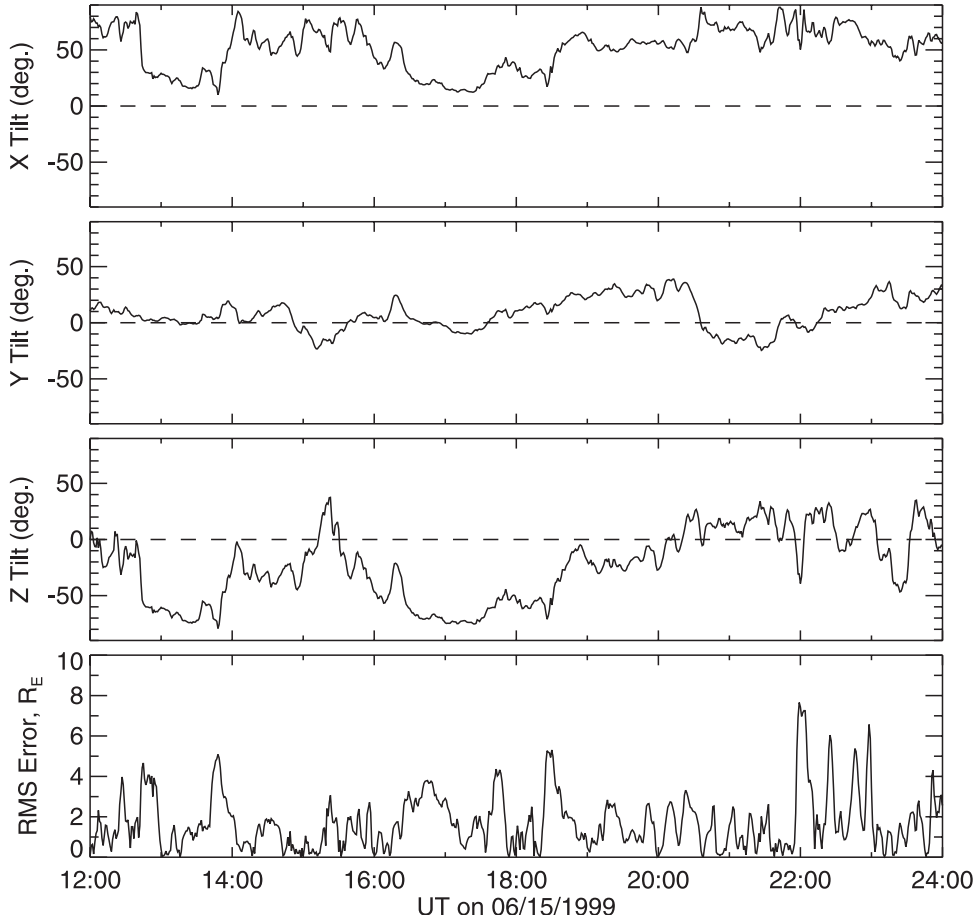

Figure 12. Graph of IMF phase plane orientation as a function of time for the case on June 15, 1999. The format is the same as in Figure 11.

not consistent. Results presented here shed a new light on the subject. Presumed trigger events may arrive at the magnetosphere much earlier or later than what was expected. Rigorous application of the technique described here can be used to help either definitively confirm or nullify the northward-turning hypothesis.

[39] How to interpret or make sense of the variable tilts is a matter of conjecture. To begin with, the planar phase fronts are certainly approximations to large-scale, curved or undulating structures in the IMF. The orientation of the local surface normal changes as the curved surfaces move by. What we observe has similarities to the planar magnetic structures described by *Nakagawa et al.* [1989], but on a much smaller spatial and temporal scale. *Nakagawa et al.* [1989, p. 11,774] interpreted their PMS events "as tongues of field lines or magnetic islands newly extended from the Sun or produced in interplanetary space." It is possible that the structures originating at the surface of the Sun to which *Nakagawa et al.* attributed the PMS produce magnetic field line structures near 1 AU at a multitude of scales.

[40] Our findings have obvious implications for basic space-weather predictions. There had been some doubts about the reliability of IMF measurements at L_1 halo orbits for predicting effects at the Earth. Our findings strengthen confidence in our ability to predict geospace environments based on upstream measurements. There remains however a serious problem with this capability, in that there is an uncertainty in the timing of events. Times when an L_1 monitor is offset from the Earth-Sun line in the Z direction likely introduce worse timing errors than offsets in the Y direction; this conclusion is based on the three-dimensional phase plane pictures and the delay times from ACE to the other satellites when the targets were offset from ACE in the Z direction. Obviously, the multiple satellite time lag technique that is used in this paper cannot now be used for making predictions, as presently there is only one satellite transmitting solar wind data in real time. It would be ideal if the phase front orientation could be determined using real-time data from a single spacecraft in an L_1 orbit, or even closer to the Sun. As mentioned above, we have made some progress along these lines with the minimum-variance technique, to be the subject of a separate paper. We suggest here that the ideal solution would be to place three monitors at L_1, spaced 120° apart in their halo orbit so that tilts in the phase fronts can be determined. ACE is a research satellite, yet by its current use within NOAA and DoD forecast centers, it has demonstrated the need for operational weather satellites at L_1, and having three would also eliminate vulnerability to a single-point failure.

[41] **Acknowledgments.** This research was supported by NASA grant NASW-99004 to Mission Research Corporation through the ACE Guest Investigator program. We especially thank the principal investigators and associates who have supplied data from the four satellites. R. Lepping is the

Principal Investigator for the magnetometer instrument on Wind. Geotail magnetic field data were provided by S. Kokubun and T. Nagai through DARTS at the Institute of Space and Astronautical Science (ISAS) in Japan. Collection and analysis of solar wind plasma (SWEPAM) and magnetometer data were supported by the NASA/ACE program.

[42] Lou-Chuang Lee and Chin S. Lin thank two reviewers for their assistance in evaluating this paper.

References

Collier, M. R., J. A. Slavin, R. P. Lepping, A. Szabo, and K. Ogilvie, Timing accuracy for the simple planar propagation of magnetic field structures in the solar wind, *Geophys. Res. Lett.*, *25*, 2509, 1998.

Collier, M. R., A. Szabo, J. A. Slavin, R. P. Lepping, and S. Kokubun, IMF length scales and predictability: The two length scale medium, *Int. J. Geomagn. Aeron.*, *2*, 3, 2000.

Coplan, M. A., F. Ipavich, J. King, K. W. Ogilvie, D. A. Roberts, and A. J. Lazarus, Correlation of solar wind parameters between SOHO and Wind, *J. Geophys. Res.*, *106*, 18,615, 2001.

Crooker, N. U., G. L. Siscoe, C. T. Russell, and E. J. Smith, Factors controlling degree of correlation between ISEE 1 and ISEE 3 interplanetary magnetic field measurements, *J. Geophys. Res.*, *87*, 2224, 1982.

Farrugia, C. J., M. W. Dunlop, F. Geurts, A. Balogh, D. J. Southwood, D. A. Bryant, M. Neugebauer, and A. Etemadi, An interplanetary planar magnetic structure oriented at a large (−80 deg) angle to the Parker Spiral, *Geophys. Res. Lett.*, *17*, 1025, 1990.

Lyons, L. R., G. T. Blanchard, J. C. Samson, R. P. Lepping, T. Yamamoto, and T. Moretto, Coordinated observations demonstrating external substorm triggering, *J. Geophys. Res.*, *102*, 27,039, 1997.

Maynard, N. C., et al., Driving dayside convection with northward IMF: Observations by a sounding rocket launched from Svalbard, *J. Geophys. Res.*, *105*, 5245, 2000.

Maynard, N. C., G. L. Siscoe, B. U. Ö. Sonnerup, W. W. White, K. D. Siebert, D. R. Weimer, G. M. Erickson, J. A. Schoendorf, D. M. Ober, and G. R. Wilson, Response of ionospheric convection to changes in the interplanetary magnetic field: Lessons from a MHD simulation, *J. Geophys. Res.*, *106*, 21,429, 2001a.

Maynard, N. C., W. J. Burke, P.-E. Sandholt, J. Moen, D. M. Ober, M. Lester, and A. Egeland, Observations of simultaneous effects of merging in both hemispheres, *J. Geophys. Res.*, *106*, 24,551, 2001b.

McComas, D. J., S. J. Bame, P. Barber, W. C. Feldman, J. L. Phillips, and P. Riley, Solar wind electron, proton, and alpha monitor (SWEPAM) on the Advanced Composition Explorer, *Space Sci. Rev.*, *86*, 563, 1998.

Nakagawa, T., A. Nishida, and T. Saito, Planar magnetic structures in the solar wind, *J. Geophys. Res.*, *94*, 11,761, 1989.

Paularena, K. I., G. N. Zastenker, A. J. Lazarus, and P. A. Dalin, Solar wind plasma correlations between IMP-8, INTERBALL-1, and Wind, *J. Geophys. Res.*, *103*, 14,601, 1998.

Press, W. H., B. P. Flannery, S. A. Teukolsky, W. T. Vetterling, *Numerical Recipes: The Art of Scientific Computing*, 818 pp., Cambridge Univ. Press, New York, 1986.

Richardson, J. D., and K. I. Paularena, The orientation of plasma structure in the solar wind, *Geophys. Res. Lett.*, *25*, 2097, 1998.

Richardson, J. D., and K. I. Paularena, Plasma and magnetic field correlations in the solar wind, *J. Geophys. Res.*, *106*, 239, 2001.

Richardson, J. D., F. Dasevisky, and K. I. Paularena, Solar wind plasma correlations between L1 and Earth, *J. Geophys. Res.*, *103*, 14,619, 1998.

Ridley, A. J., Estimations of the uncertainty in timing the relationship between magnetospheric and solar wind processes, *J. Atmos. Sol. Terr. Phys.*, *4*, 1, 2000.

Ridley, A. J., G. Lu, C. R. Clauer, and V. O. Papitashvili, A statistical study of the ionospheric convection response to changing interplanetary magnetic field conditions using the assimilative mapping of ionospheric electrodynamics technique, *J. Geophys. Res.*, *103*, 4023, 1998.

Russell, C. T., G. L. Siscoe, and E. J. Smith, Comparison of ISEE 1 and 3 interplanetary magnetic field observation, *Geophys. Res. Lett.*, *7*, 381, 1980.

Russell, C. T., et al., The interplanetary shock of September 24, 1998: Arrival at Earth, *J. Geophys. Res.*, *105*, 25,143, 2000.

Sonnerup, B. U. Ö., Magnetopause reconnection rate, *J. Geophys. Res.*, *79*, 1546, 1974.

Sonnerup, B. U. Ö., and L. J. Cahill, Magnetopause structure and attitude from Explorer 12 observations, *J. Geophys. Res.*, *72*, 171, 1967.

Sonnerup, B. U. Ö., and M. Scheible, Minimum and maximum variance analysis, in *Analysis Methods for Multi-Spacecraft Data*, edited by G. Paschmann and P. W. Daly, Int. Space Sci. Inst., Bern, 1998.

Tsurutani, B., and D. N. Baker, Substorm warnings: An ISEE-3 real time data system, *Eos Trans. AGU*, *60*, 702, 1979.

Turner, J. M., and G. L. Siscoe, Orientations of "rotational" and "tangential" discontinuities in the solar wind, *J. Geophys. Res.*, *76*, 1816, 1971.

W. J. Burke, Air Force Research Laboratory Space Vehicles Directorate, 29 Randolph Road, Hanscom AF Base, MA 01731, USA.

M. R. Collier, Laboratory for Extraterrestrial Physics, NASA/GSFC, Greenbelt, MD 20771, USA.

N. C. Maynard, D. M. Ober, and D. R. Weimer, Mission Research Corporation, 589 West Hollis St., Suite 201, Nashua, NH 03062, USA. (dweimer@mrcnh.com)

D. J. McComas, Southwest Research Institute, P.O. Drawer 28510, San Antonio, TX 78228-0510, USA.

N. F. Ness and C. W. Smith, Bartol Research Institute, University of Delaware, Newark, DE 19716-4793, USA.

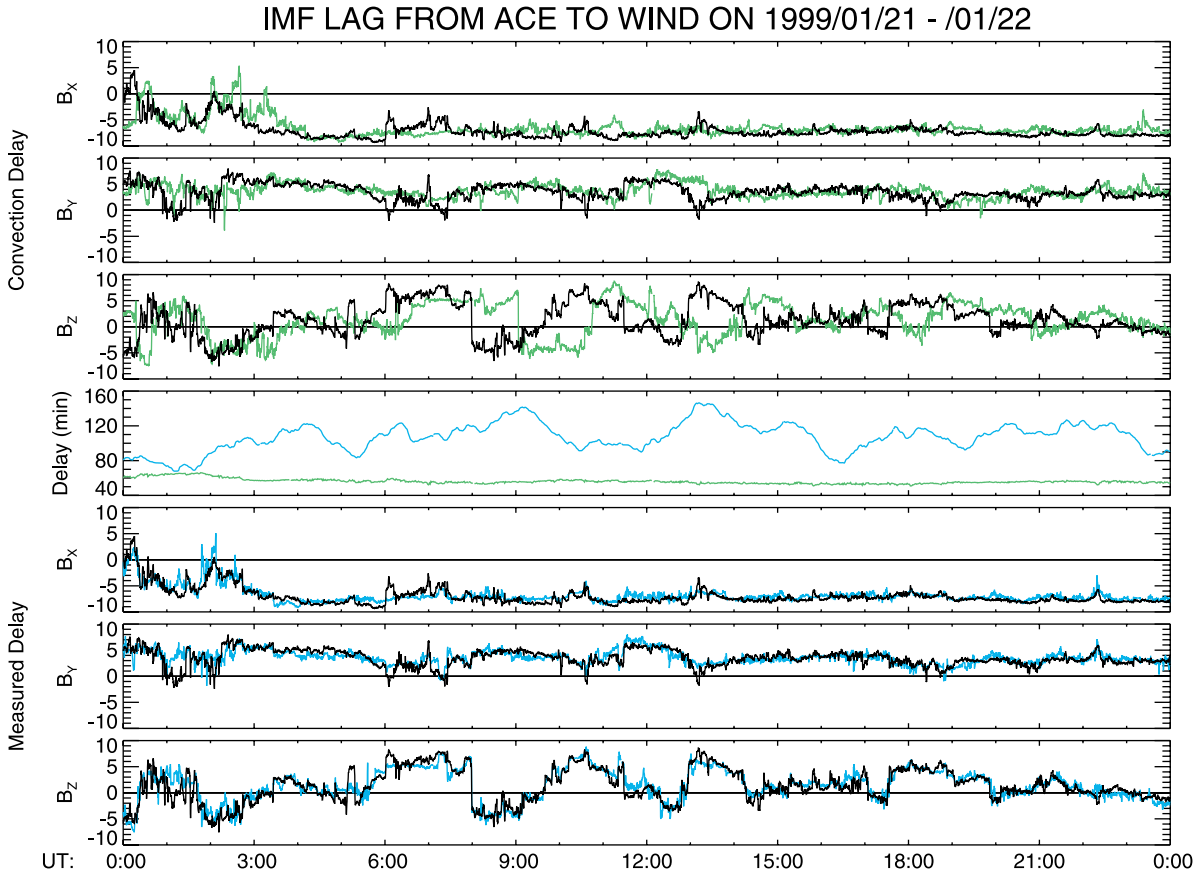

Figure 1. Interplanetary magnetic field (IMF) measured with the ACE and Wind satellites on January 21, 1999. The black lines in the three top and bottom panels show the ACE data. The green lines in the top three panels show the Wind data, with the measurements shifted in time according to the value of the advection delay, shown as the green line in the middle panel. The blue lines in the bottom three panels show the same data from Wind shifted in time by a variable amount that results in the best agreement with the ACE data. The lag time that produces this agreement is called the "measured delay," and is shown as the blue line in the middle panel.

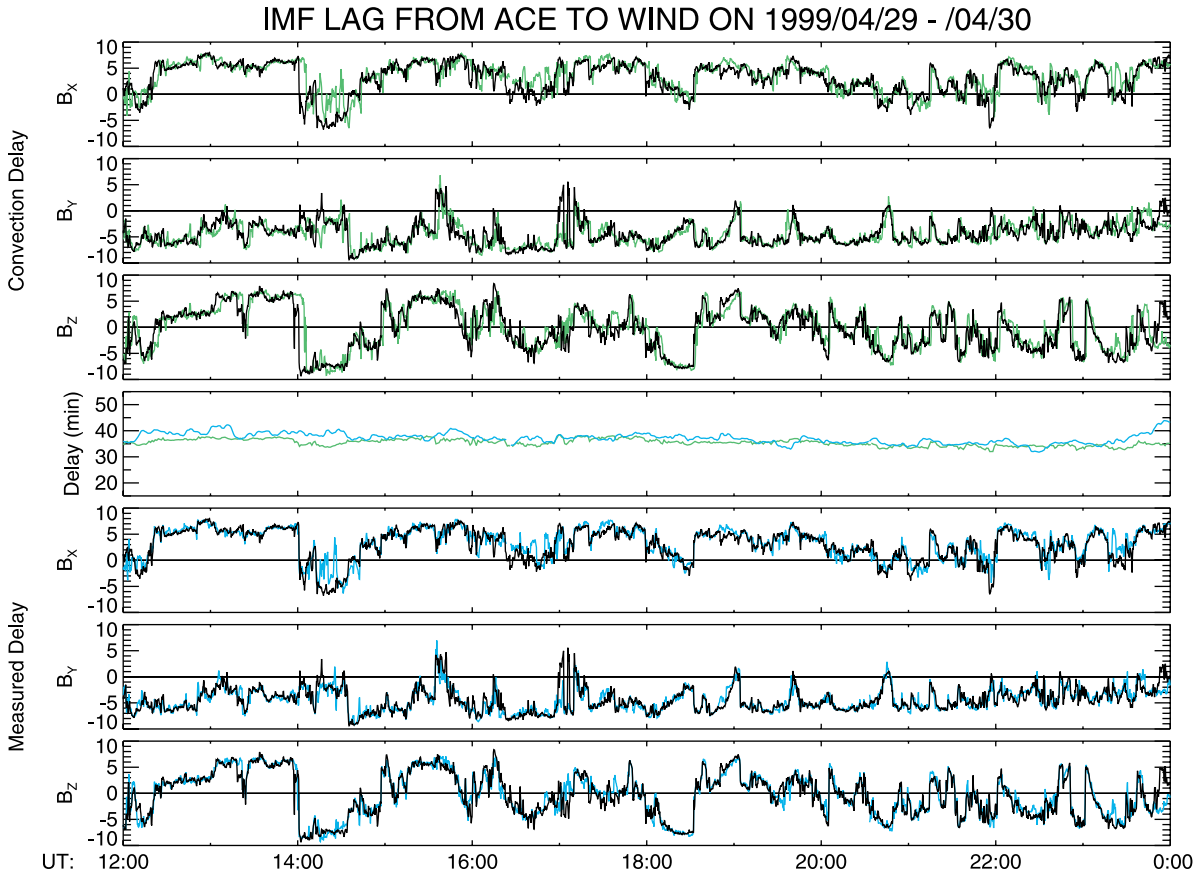

Figure 3. IMF measured with the ACE and Wind satellites on April 29, 1999. The format is the same as in Figure 1.

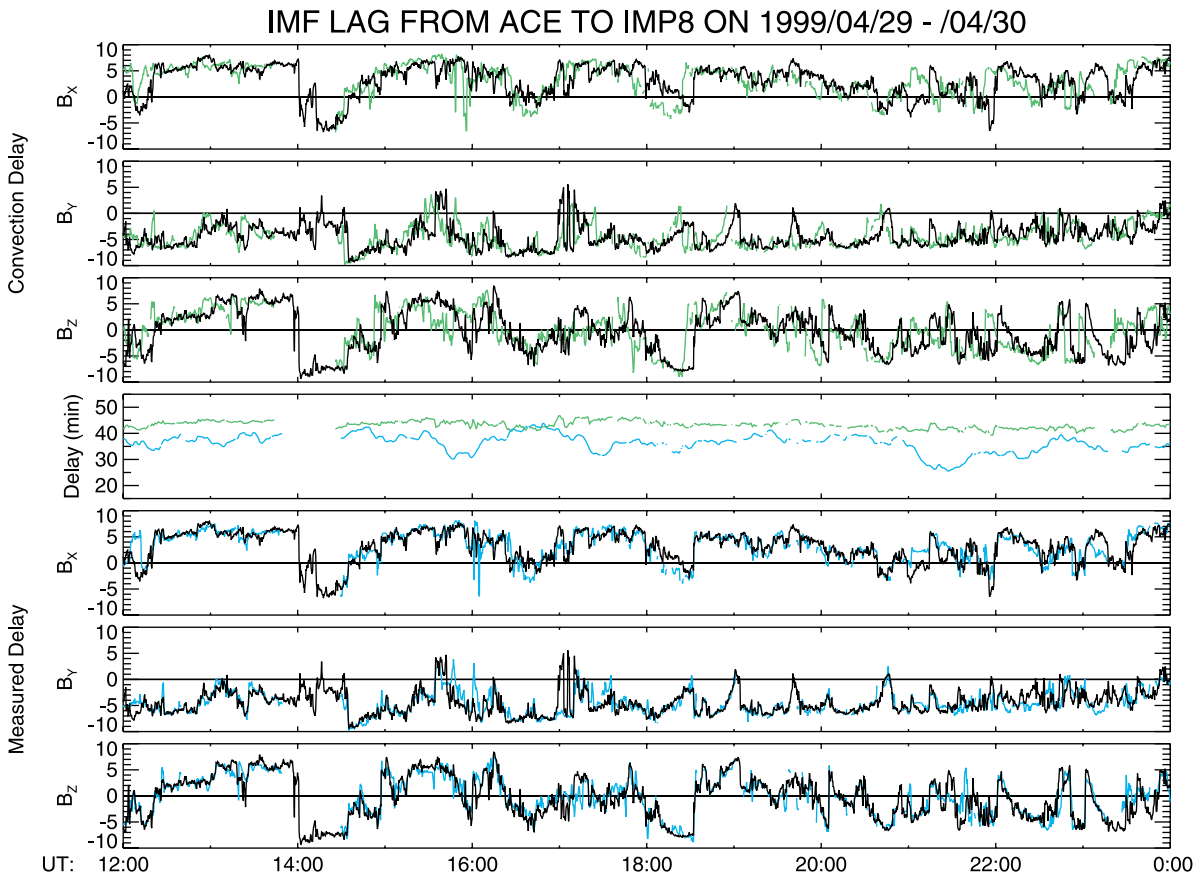

Figure 4. IMF measured with the ACE and IMP-8 satellites on April 29, 1999. The format is the same as in Figure 1, with the green and blue lines now showing the IMP-8 data. The gaps in the green and blue lines indicate where there were gaps in the IMF measured with IMP-8.

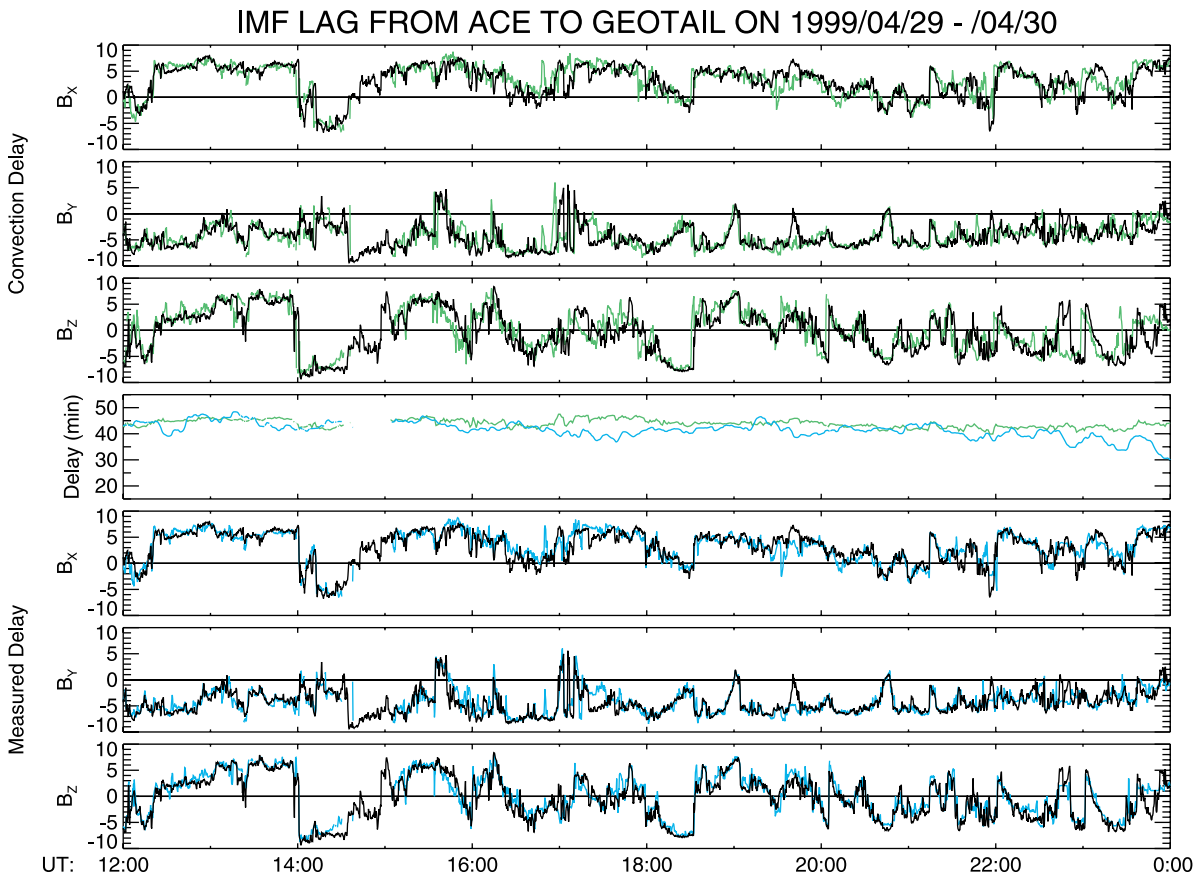

Figure 5. IMF measured with the ACE and Geotail satellites on April 29, 1999.

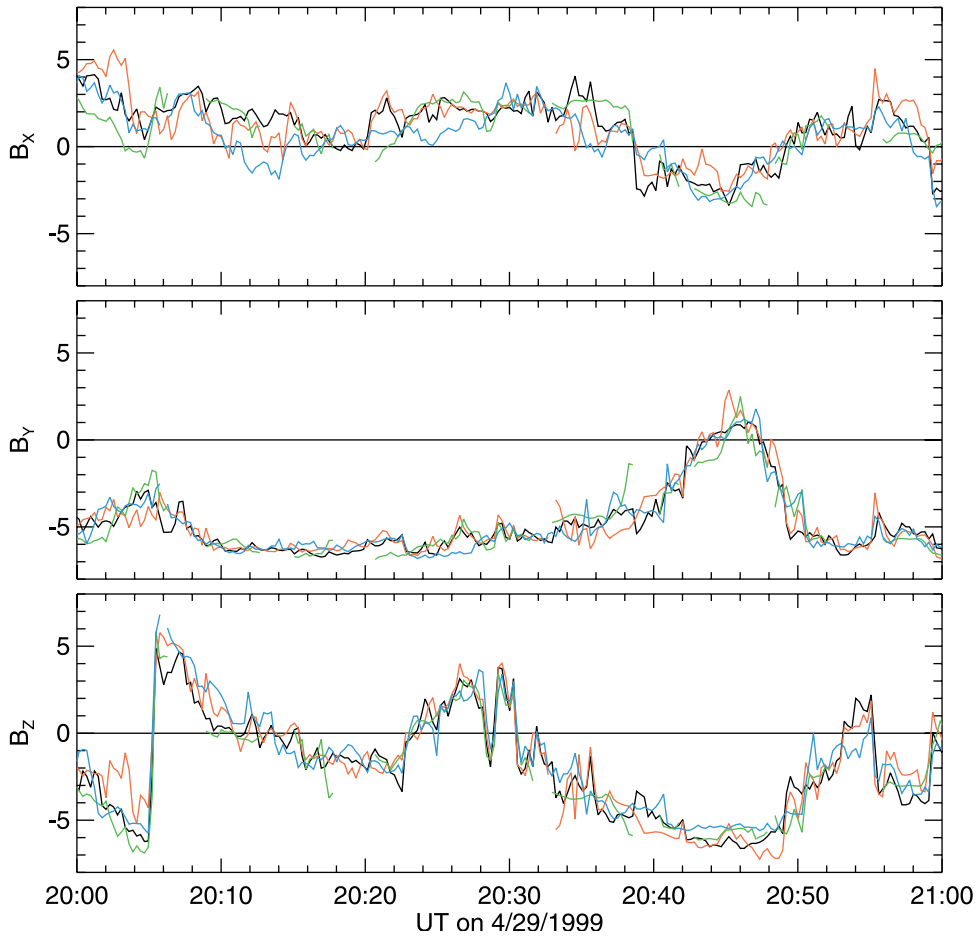

Figure 6. High-resolution graph of the IMF measured with all four satellites for a one hour interval on April 29, 1999. The data have been shifted according to the "measured" time delays, and are plotted on the same timescale as the ACE data, which are not shifted. The black, red, green, and blue lines show the data from ACE, Wind, IMP-8, and Geotail respectively.

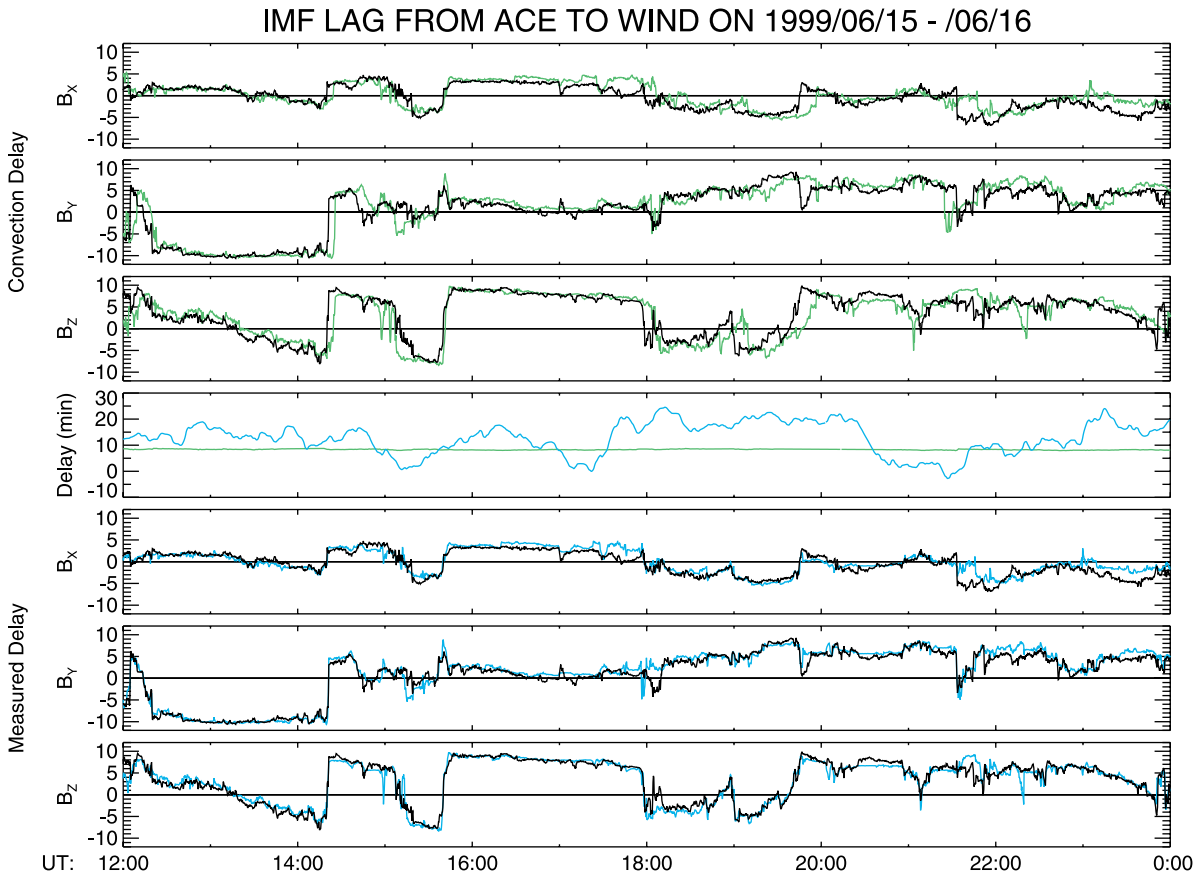

Figure 7. IMF measured with the ACE and Wind satellites on June 15, 1999.

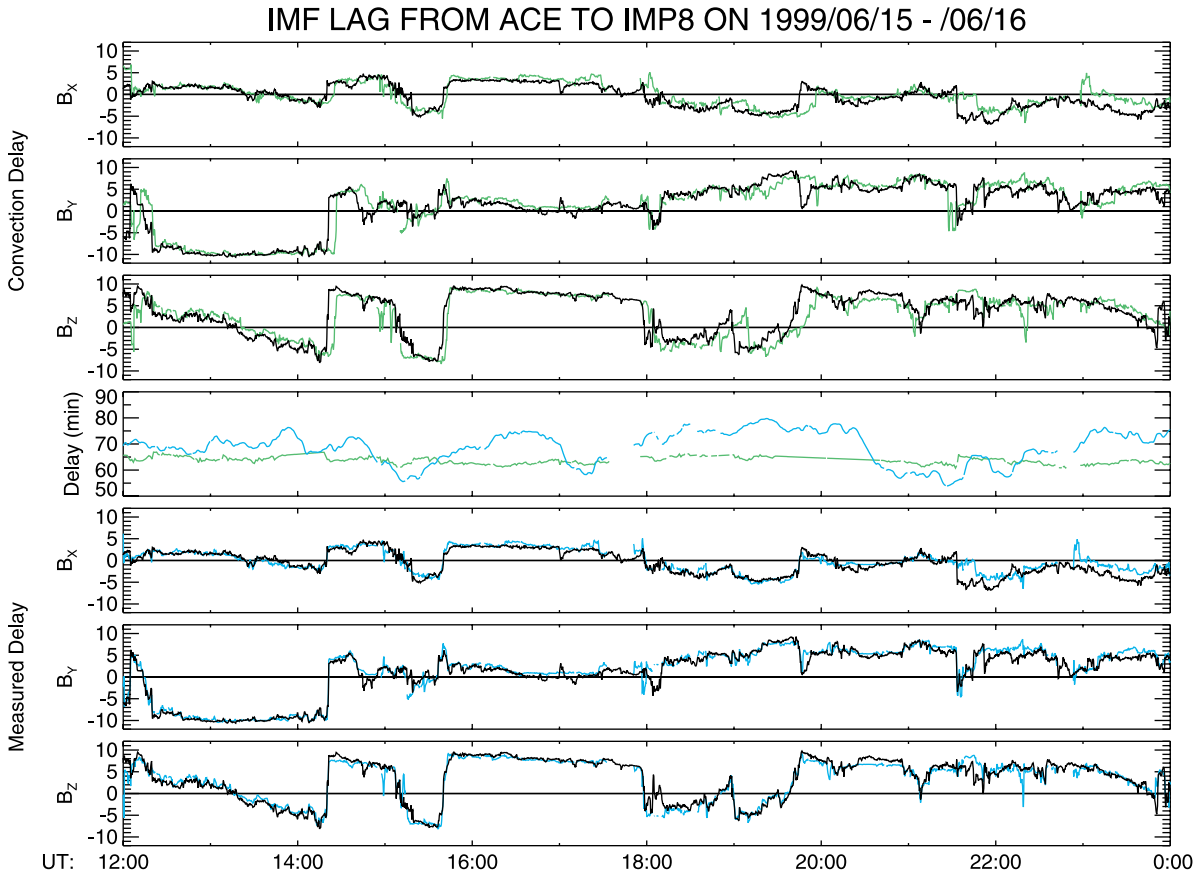

Figure 8. IMF measured with the ACE and IMP-8 satellites on June 15, 1999.

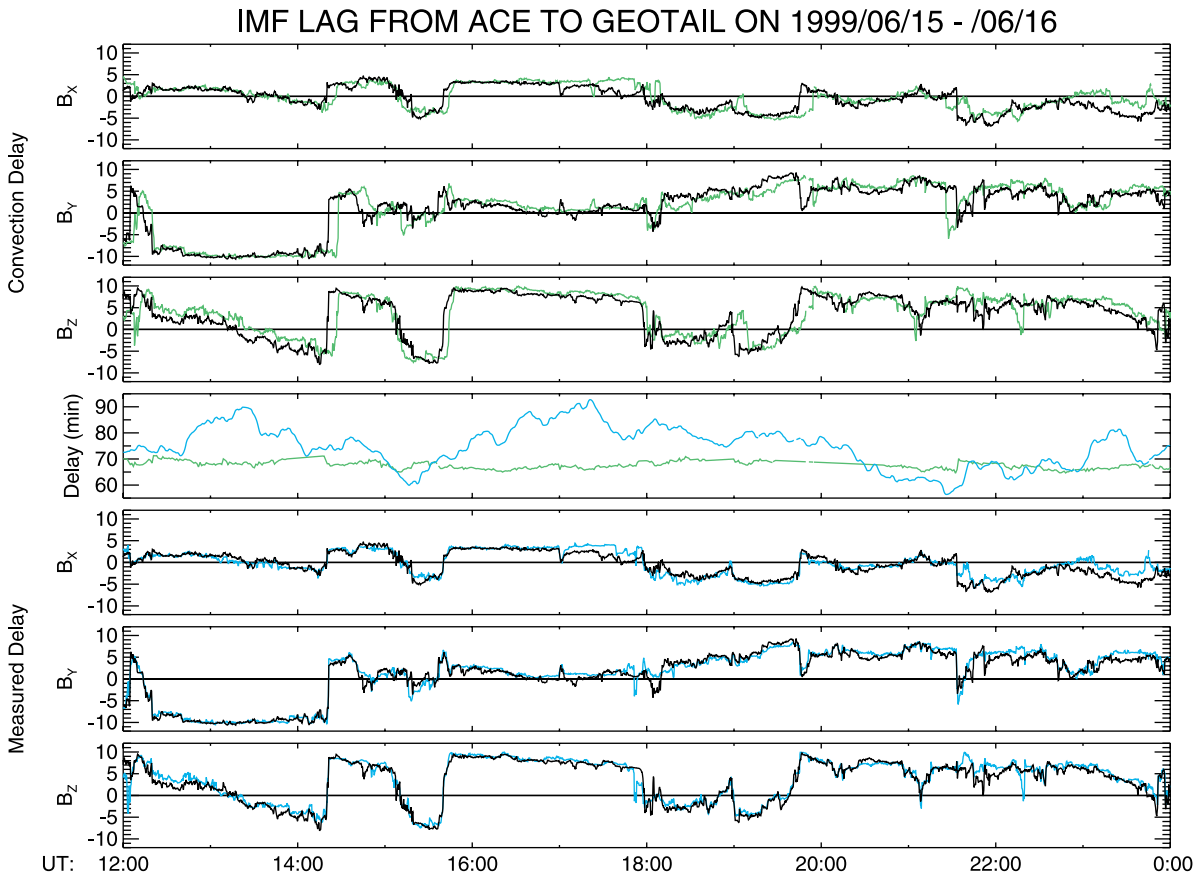

Figure 9. IMF measured with the ACE and Geotail satellites on June 15, 1999.

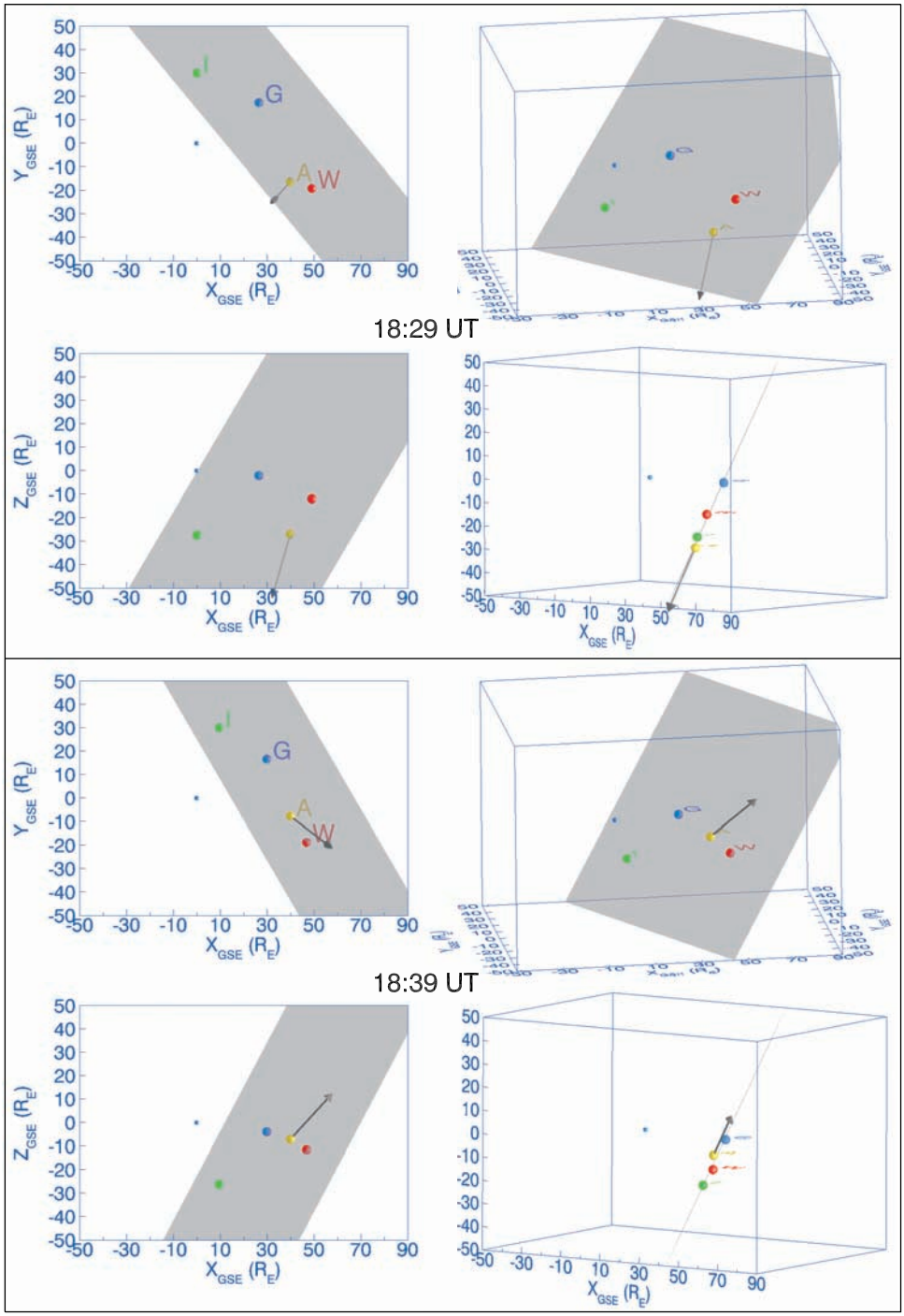

Figure 10. Three-dimensional views of the IMF phase plane orientation at two moments in time on April 29, 1999. The top four pictures show the phase plane from different viewpoints at 1829 UT, and the bottom four pictures show the same views 10 min later, at 1839 UT. The four colored spheres show the "virtual" locations of the four satellites, with the ACE satellite shifted forward up to X = 40 R_E and the others shifted according to the measured delay times and solar wind velocity, compensated for the ACE shift. All shifts are along the velocity vector, measured at ACE. The spheres are labeled with the first initial of each satellite. These spheres are drawn with a diameter of 4 R_E. For reference, a blue sphere representing the Earth is shown at the origin. The arrow at the ACE location has a fixed length and points in the direction of the IMF vector measured at ACE. The phase plane orientation remains nearly the same while the vector reverses direction.